# NATIONAL ADVISORY COMMITTEE FOR AERONAUTICS

TECHNICAL NOTE

No. 1378

## PRELIMINARY INVESTIGATION AT LOW SPEED OF DOWNWASH CHARACTERISTICS OF SMALL-SCALE SWEPTBACK WINGS

By Paul E. Purser, M. Leroy Spearman, and William R. Bates

Langley Memorial Aeronautical Laboratory
Langley Field, Va.

Washington
July 1947

NATIONAL ADVISORY COMMITTEE FOR AERONAUTICS

TECHNICAL NOTE NO. 1378

# PRELIMINARY INVESTIGATION AT LOW SPEED OF DOWNWASH CHARACTERISTICS OF SMALL-SCALE SWEPTBACK WINGS

By Paul E. Purser, M. Leroy Spearman, and William R. Bates

## SUMMARY

A preliminary investigation has been made at low speed of the downwash behind various small-scale sweptback wings. The wing configurations for which data were obtained covered aspect ratios from 2.5 to 4.0, sweepback angles from 32.5° to 40°, and ratios of root chord to tip chord from 0.62 to 2.06.

The data showed that for the higher tails and shorter tail lengths behind each of the wings in the wing-tail combinations tested fairly large variations occurred in the rate of change of downwash angle with angle of attack $d\epsilon/d\alpha$ at high angles of attack with resulting large changes in the longitudinal stability of the wing-tail combinations. In general, lowering the tail to a position near the extended chord line of the wing and increasing the tail length caused improvement of the stability as characterized by decreases in $d\epsilon/d\alpha$ and by decreases in the variation of $d\epsilon/d\alpha$ with angle of attack.

Increasing the wing aspect ratio caused a reduction in $d\epsilon/d\alpha$ and improved the tail contribution to the stability. Increasing the ratio of wing root chord to tip chord caused increases in the rate of change of downwash angle with angle of attack for the low lift range.

The use of trailing-edge flaps caused a slight increase in $d\epsilon/d\alpha$ and caused an increment of downwash angle at low angles of attack about the same as would be expected for unswept wings. Leading-edge slats reduced the variation of $d\epsilon/d\alpha$ at high lift coefficients and generally resulted in improvement of the stability.

Values of downwash angle computed from design charts for unswept wings given in NACA Reports No. 648 and 711 agreed fairly well with experimental data at low lift coefficients provided the computations were based on the aspect ratio and span of an unswept wing having the same panels as the sweptback wing.

## INTRODUCTION

The analysis of reference 1 shows that the use of sweptback wings for high-speed aircraft can greatly extend the range of flight Mach number attainable before the onset of serious compressibility effects on the wings. The National Advisory Committee for Aeronautics is therefore attempting to supply design data on the characteristics of swept wings. For the low-speed range in which the disadvantages inherent in the use of high degrees of sweep appear to be greatest, the Langley Laboratory of the NACA has supplied such data on the low-speed stability and control characteristics of sweptback wings in references 2 and 3 and has provided a collection and analysis of static longitudinal stability characteristics of sweptback wings in reference 4.

The analysis of reference 4 shows that the static longitudinal stability of isolated wings, particularly near the stall, is greatly dependent upon the aspect ratio and sweepback angle. A summary chart based on these two parameters is presented in reference 4 for use in determining stable and unstable combinations of sweep and aspect ratio. Other data presented in reference 4 indicate, however, that the problem of obtaining adequate longitudinal stability for wing-tail combinations is more complex than that for wings alone because of apparently large and unpredictable downwash changes in the region of the tail surfaces.

As an extension to the work of reference 4, the present paper provides a collection and brief analysis of downwash measurements made behind various sweptback wings. The data were obtained from tuft observations and force tests of wing-tail combinations in the Langley 7- by 10-foot tunnel.

## COEFFICIENTS AND SYMBOLS

$C_L$ lift coefficient (Lift/qS)

$C_{L_t}$ isolated-tail lift coefficient (Lift of isolated tail/$qS_t$)

$C_D$ drag coefficient (Drag/qS)

$C_m$ pitching-moment coefficient about quarter chord of wing mean aerodynamic chord (Pitching moment/$qSc'$)

q dynamic pressure, pounds per square foot $\left(\rho\frac{V^2}{2}\right)$

$\rho$ mass density of air, slugs per cubic foot

$V$ air velocity, feet per second

$S$ wing area, square feet

$S_t$ tail area, square feet

$c$ airfoil section chord, feet

$c'$ airfoil mean aerodynamic chord, feet $\left(\frac{2}{S}\int_0^{b/2} c^2\,dy\right)$

$c_R$ airfoil root chord, feet

$c_T$ airfoil tip chord, feet

$\Lambda_{c/4}$ angle of sweepback of line of quarter-chord points of airfoil, degrees

$A$ wing aspect ratio $(b^2/S)$

$A_t$ tail aspect ratio $\left(b_t^2/S_t\right)$

$b$ wing span, feet

$b_t$ tail span, feet

$\alpha$ angle of attack of wing chord line, degrees

$\alpha_t$ angle of attack of tail chord line, degrees

$\epsilon$ angle of downwash, determined from tuft surveys, degrees

$\epsilon'$ effective angle of downwash, determined from force-test data, degrees

$i_t$ tail setting with respect to wing chord line, positive when trailing edge moves down, degrees

$q_t$ effective dynamic pressure at tail, pounds per square foot

$l_t$ tail length, distance in chord plane from quarter-chord point of wing mean aerodynamic chord to quarter-chord point of tail mean aerodynamic chord or to a point in survey plane equivalent to quarter-chord point of tail mean aerodynamic chord, feet

$h_t$ tail height, vertical distance from wing chord plane to tail chord plane or to point in survey plane, feet

$y$ spanwise distance from plane of symmetry, feet

$n_p$ neutral point

## MODELS AND APPARATUS

### Models

Details of the models tested are shown in figures 1 to 7. All the wings and tails were made of laminated mahogany. The tails of models A to D were mounted on a 2- by 4-inch pine fuselage by means of the fittings shown in figure 8.

### Survey Apparatus

Downwash surveys for models D, E, and F were made with the tuft apparatus shown in figure 9. For models B and C the wires extended from the tunnel floor to the ceiling and from $\frac{y}{b/2} = 0$ to $\frac{y}{b/2} = 1.0$. The row of wires supporting the tufts was swept back 40° and photographs (see fig. 10) were taken from the side of the tunnel at an angle of 90° to the air stream. The photographs were enlarged to approximately one-half full-size and the tuft angles were read by using the vernier protractor of a drafting machine.

## TESTS AND RESULTS

### Test Conditions

The following table summarizes the test conditions for the various models in the Langley 7- by 10-foot tunnel:

| Model | Dynamic pressure (lb/sq ft) | Test Reynolds number | Turbulence factor |
|---|---|---|---|
| A, B, and C | 17.16 | $0.834 \times 10^6$ | 1.6 |
| D | 16.37 | .974 | 1.6 |
| E | 16.37 | .820 | 1.6 |
| F | 16.37 | .800 | 1.6 |
| Isolated tails | 16.37 | .410 | 1.6 |

## Corrections

Tares.- The model force-test data have not been corrected for tares. The data for the isolated tails of models A, B, C, and D have been approximately corrected for tares by adjusting the angle of zero lift to $-3.8^{\circ}$. This angle is a corrected value based on tests data for unswept Clark Y airfoils multiplied by the cosine of $40^{\circ}$ to account approximately for sweep effects.

The downwash angles determined from tuft surveys for the symmetrical airfoils (models B and C) were approximately corrected for tares by subtracting the downwash angles measured at an angle of attack of zero from the downwash angles measured at all angles of attack. For the cambered airfoils (models D, E, and F) the tare downwash angles were determined from tuft measurements made with the models removed but with the model support strut installed in the tunnel.

Jet-boundary effects.- The various jet-boundary corrections applied to the force-test data are presented in table I. These corrections are standard values developed for unswept wings (see reference 5) and for the present tests were based on the actual aspect ratio and area of each sweptback wing.

Within the limits of applicability of the jet-boundary corrections developed for unswept wings to tests of swept wings, the effective downwash angles determined from the corrected force-test data are also corrected for jet-boundary effects.

No jet-boundary corrections have been applied to the downwash angles measured by tufts for any models, but the angles of attack presented with the tuft-survey data are also uncorrected in order that the values of $d\epsilon/d\alpha$ obtained from these data might be more nearly correct.

## Tests and Presentation of Results

Force tests.- Force tests of all models were made through the angle-of-attack range from about $-4^{\circ}$ to the stall angle. For models A to D tests were made with the tail removed and with the tail set at approximately $0^{\circ}$ and $-6^{\circ}$ relative to the wing chord line at each of the positions shown in figures 1 to 4.

For models A to D the values of effective downwash angle $\epsilon'$ and dynamic-pressure ratio were computed from tail-off, tail-on, and isolated-tail tests by a method of successive approximations which takes into account the nonlinearity of the isolated-tail lift curve.

Downwash surveys.- The downwash surveys behind models B and C with the tail removed and behind the wings of models D, E, and F were made through the angle-of-attack range from 0° to 20° in the survey planes shown in figures 2, 3, 4, 6, and 7. Since the groups of tufts were fixed in space, the survey planes were located differently with respect to the model for each angle of attack, as shown in figure 11. The data are shown located with respect to the chord plane, and the fact that the survey planes did not remain perpendicular to the chord plane was ignored because of the relatively small variation of downwash with longitudinal location in the survey region.

Presentation of results.- The data are presented in figures 12 to 30 in three general groups: force-test data, tuft surveys, and analysis plots and are indexed in table II.

## DISCUSSION

### General

The force-test data, particularly data in figures 12(a), 13(a), 14(a), and 15(a), and the tuft surveys (figs. 20 to 24) indicate that for high tails and short tail lengths behind each of the wings tested for the present investigation, the variation of downwash angle with angle of attack undergoes rather large changes at high values of lift coefficient ($C_L > 0.6$). These changes in $d\epsilon/d\alpha$ usually occur at angles of attack near the angles at which changes occur also in the wing lift, pitching-moment, and drag characteristics. Tuft observations of the flow at the wing surface show marked changes in the flow pattern at these same angles of attack and indicate a general shift of lift load toward the root section. That such a shift of load occurs for sweptback wings is shown by the data of reference 6 and in tests made in the Langley 8-foot high-speed tunnel. The changes in $d\epsilon/d\alpha$ that occur at high lift coefficients therefore are probably a result of the increased load carried by the root section.

Data obtained in the Langley 19-foot pressure tunnel show that the changes in air flow, lift, pitching moment, and drag that occur at low Reynolds numbers at values of lift coefficient of 0.6 and higher are reduced or delayed to higher angles of attack by increases in the Reynolds number. It is to be expected, therefore, that the data presented herein, which were all obtained in tests at low Reynolds numbers, may tend to overemphasize the changes in $d\epsilon/d\alpha$. The actual changes occurring on full-size aircraft probably would be less marked and would occur at higher values of lift coefficient than do the changes presented in the present paper. The data obtained

in the 19-foot pressure tunnel, however, show relatively small effects of Reynolds number at low lift coefficients; therefore the low Reynolds number of the present tests should have little effect on the validity of the present data at low lift coefficients.

Since analysis of the data involves a discussion of both force-test measurements and tuft surveys, a comparison of the results obtained by these two methods is shown in figures 25 and 26. An incremental difference exists between the values of downwash angle obtained by the two methods that is probably caused by tares; however, the slopes of the curves are very nearly the same. The tuft-survey data presented are values for a station at the midpoint of the tail semispan and no attempt was made to account for spanwise variations of downwash angle and tail lift distribution. As noted in the section entitled "Corrections" neither the downwash angles nor the angles of attack from the tuft tests have been corrected. The corrections to both downwash angle and angle of attack are of the same sense and order of magnitude, however, and as shown by table I the corrections to angle of attack are relatively small for all the models tested.

## Effect of Aspect Ratio

The effect of wing aspect ratio on the effective downwash angle behind sweptback wings is shown in figure 27. The aspect ratios of the wing and tail were reduced by the same amount so that the tail for each model would be affected by relatively the same portion of the wing. The physical positions of the wing and tail remained unchanged when the aspect ratio was changed. The data of figure 27 indicate that a reduction in aspect ratio produces an increase in the value of $d\epsilon/d\alpha$, with the effect being less marked for the longer tail lengths.

For all the wings tested the changes in $d\epsilon'/d\alpha$ resulting from a change in aspect ratio are of the order of magnitude obtained for unswept wings from the charts of references 7 and 8. The measured values of $d\epsilon'/d\alpha$ for a given sweptback wing, however, are less than would be calculated for an unswept wing of the same aspect ratio and more nearly approach the values calculated for an unswept wing having the same panels as the swept wing. This result is illustrated in figure 30 in which measured values of $d\epsilon'/d\alpha$ for the low lift-coefficient range are compared with values computed from the charts of references 7 and 8 by three different methods:

(1) Actual values of A and b obtained on the swept wings were used in the charts.

(2) Actual value of $b$ was used but value of $A$ was multiplied by the factor $\frac{1}{\cos^2\Lambda_{c/4}}$

(3) Value of $b$ was multiplied by $\frac{1}{\cos\Lambda_{c/4}}$ and value of $A$ was multiplied by $\frac{1}{\cos^2\Lambda_{c/4}}$

Method (3) is equivalent to basing the computations on an unswept wing having the same panels as the swept wings. This method, although strictly empirical and having no theoretical basis, gave the closest agreement between experimental and computed values of $d\epsilon'/d\alpha$. Computations of $d\epsilon'/d\alpha$ made by method (3) for four complete models have also shown good agreement with experimental values obtained in the Langley 300 MPH 7- by 10-foot tunnel.

## Effect of Taper Ratio

The only directly comparable data on the effects of taper ratio were obtained for models D and E. These data are compared in figure 28, which shows that for the low lift range the model with conventional taper $\left(\frac{c_R}{c_T} = 2.04\right)$ has greater downwash angle than the wing with inverse taper $\left(\frac{c_R}{c_T} = 0.617\right)$ as would be expected from the design charts of references 7 and 8. The data of figure 28 indicate that in general a more uniform variation of $\epsilon$ with angle of attack is obtained for the model with conventional taper. At $0.2\frac{b}{2}$ above the chord line, for example, the model of conventional taper shows a fairly uniform increase in downwash angle with angle of attack, whereas the wing of inverse taper shows a particularly rapid increase in downwash angle between angles of attack of 12° and 16°. This result might be expected since the force-test data (figs. 16 and 17) also show smaller departures from linearity for the lift and pitching-moment curves for the conventional-taper model as compared with the curves for the inverse-taper wing.

## Effect of Tail Span and Position

Tail span.- The downwash data for the wing of model D (inverse taper) indicate that in general the average value of $d\epsilon/d\alpha$ increases

as the tail span increases. (See fig. 21.) This condition is probably a result of an increased lift load carried by the tips of the sweptback inverse-taper wing as the angle of attack increases. For the wings with conventional taper - models E and F shown in figures 23 and 24, respectively - a similar increase in the average value of $d\epsilon/d\alpha$ occurs at low angles of attack for tail spans as large as about $0.5\frac{b}{2}$. For higher angles of attack and for tail spans greater than about $0.5\frac{b}{2}$, the data generally indicate a decrease in $d\epsilon/d\alpha$ with increasing tail span, because at high angles of attack the tip stalling tendencies of sweptback wings reduce the tip lift load and because at all angles of attack conventional taper has a relieving effect on the lift load at the tip.

For the untapered wings (models B and C) the spanwise variation of $d\epsilon/d\alpha$ is small until angles of attack approaching the stall angle are reached. (See figs. 20 and 29.) At these high angles of attack, the data for $b_t = 0.50b$ indicate an increase in $d\epsilon/d\alpha$ whereas the data for $b_t = 0.80b$ indicate a decrease (fig. 29). The difference in effective downwash angle for the two tail spans is again probably caused by an inboard shift of the lift load for sweptback wings at high angles of attack when the tips stall.

Tail position.- Both the tuft-survey and force-test data indicate the large effect of both the vertical and longitudinal positions of the tail on the variation of downwash angle with angle of attack in the moderate to high lift-coefficient range. For example, figures 12 to 14 show for models A, B, and C with the short tail length (position 1) an increase in $d\epsilon'/d\alpha$ and a corresponding unstable change in slope of the pitching moment near maximum lift. When the tail length is increased (position 2 for models A and B and position 3 for model C) the unstable changes in $d\epsilon'/d\alpha$ and $dC_m/dC_L$ near maximum lift are eliminated. A similar comparison of the pitching-moment and downwash data for positions 1 and 2 of models C and D (figs. 14 and 15) shows that lowering the tail to a position nearer the extended chord line of the wing tends to eliminate unstable changes in $d\epsilon'/d\alpha$ and $dC_m/dC_L$ near maximum lift. The tuft data (figs. 20 to 24) indicate that for high tail positions the value of $d\epsilon/d\alpha$ tends to increase at high angles of attack, whereas for low tail positions the opposite is true.

In general, the tail positions that are lowest and farthest rearward provide the most favorable downwash; that is, in such positions the values of $d\epsilon/d\alpha$ either remain constant or show a stabilizing decrease with increased lift coefficient. This result

tends to explain the data of reference 4 wherein the presence of a tail was shown to improve the longitudinal stability characteristics of an unstable wing and to impair the characteristics of a stable wing.

## Effect of High-Lift Devices

Trailing-edge flaps.- As shown by the data in figure 22 half-span flaps on the trailing edge of the wing of model D have the usual effect of producing an initial positive value of downwash angle at zero angle of attack and generally cause a slight increase in $d\epsilon/d\alpha$, as is indicated in reference 9. Computations made by the method of reference 7, based on an unswept wing having the same panels as the sweptback wing of model D, indicate that at $0.03\frac{b}{2}$ above the extended chord line the increment of downwash angle at $\alpha = 0$ caused by flap deflection should be about $5^{\circ}$, whereas the data of figure 22 indicate an increment of about $5.8^{\circ}$. Computations based on the actual span and aspect ratio of the sweptback wing indicated an increment of only $3.8^{\circ}$.

Wing-tip leading-edge slats.- The data of figure 22 show little effect on $d\epsilon/d\alpha$ of the addition of half-span slats at the leading edge of the wing tip of model D in the low lift-coefficient range. At higher lifts, however, the presence of the slats reduced $d\epsilon/d\alpha$ over the inner 50 percent of the span for tail positions lower than about $0.3\frac{b}{2}$ above the extended chord line and increased $d\epsilon/d\alpha$ for tail positions higher than about $0.3\frac{b}{2}$.

## CONCLUSIONS

The results of tests at low speed to determine downwash characteristics behind various small-scale sweptback wings indicated the following conclusions:

1. Rather large variations in the rate of change of downwash angle with angle of attack $d\epsilon/d\alpha$ occurred for the higher tails and shorter tail lengths behind each of the wings in the wing-tail combinations tested at high angles of attack with resulting large changes in longitudinal stability of the wing-tail combinations.

2. Extending the tail length and lowering the tail to a position near the extended chord line generally caused a decrease in $d\epsilon/d\alpha$ and improved the stability at high lift coefficients.

3. Increasing the wing aspect ratio caused a reduction in $d\epsilon/d\alpha$ and improved the tail contribution to the stability.

4. Increasing the ratio of wing root chord to tip chord caused an increase in $d\epsilon/d\alpha$ for the low lift range.

5. The use of trailing-edge flaps caused a slight increase in $d\epsilon/d\alpha$ and caused an increment in the angles of downwash at low angles of attack about the same as would be expected on an unswept wing. Leading-edge slats caused slight decreases in $d\epsilon/d\alpha$ at high lifts and improved the stability.

6. Values of downwash angle computed from design charts for unswept wings given in NACA Reports No. 648 and 711 agreed fairly well with experimental data at low lift coefficients provided the computations were based on the aspect ratio and span of an unswept wing having the same panels as the sweptback wing.

Langley Memorial Aeronautical Laboratory
National Advisory Committee for Aeronautics
Langley Field, Va., April 9, 1947

## REFERENCES

1. Jones, Robert T.: Wing Plan Forms for High-Speed Flight. NACA TN No. 1033, 1946.

2. Letko, William, and Goodman, Alex: Preliminary Wind-Tunnel Investigation at Low Speed of Stability and Control Characteristics of Swept-Back Wings. NACA TN No. 1046, 1946.

3. Lowry, John G., and Schneiter, Leslie E.: Investigation at Low Speed of the Longitudinal Stability Characteristics of a 60° Swept-Back Tapered Low-Drag Wing. NACA TN No. 1284, 1947.

4. Shortal, Joseph A., and Maggin, Bernard: Effect of Sweepback and Aspect Ratio on Longitudinal Stability Characteristics of Wings at Low Speeds. NACA TN No. 1093, 1946.

5. Gillis, Clarence L., Polhamus, Edward C., and Gray, Joseph L., Jr.: Charts for Determining Jet-Boundary Corrections for Complete Models in 7- by 10-Foot Closed Rectangular Wind Tunnels. NACA ARR No. L5G31, 1945.

6. Jacobs, W.: Druckverteilungsmessungen an Pfeilflügeln konstanter Tiefe bei symmetrischer Anströmung. UM Nr. 2052, Deutsche Luftfahrtforschung (Braunschweig), 1943.

7. Silverstein, Abe, and Katzoff, S.: Design Charts for Predicting Downwash Angles and Wake Characteristics behind Plain and Flapped Wings. NACA Rep. No. 648, 1939.

8. Gilruth, R. R., and White, M. D.: Analysis and Prediction of Longitudinal Stability of Airplanes. NACA Rep. No. 711, 1941.

9. Silverstein, Abe, Katzoff, S., and Bullivant, W. Kenneth: Downwash and Wake behind Plain and Flapped Airfoils. NACA Rep. No. 651, 1939.

TABLE I

JET-BOUNDARY CORRECTIONS APPLIED TO FORCE-TEST DATA

| Model | Jet-boundary corrections | | | |
|---|---|---|---|---|
| | $\Delta\alpha/C_L$ | $\Delta C_D/C_L^2$ | $\Delta C_m/C_L$ | |
| | | | Short tail length | Long tail length |
| A | 0.44 | 0.0076 | 0.0072 | 0.0146 |
| B | .28 | .0049 | .0080 | .0130 |
| C | .28 | .0049 | .0030 | .0080 |
| D | .53 | .0093 | .0069 | .0117 |
| E | .32 | .0057 | - - - - | - - - - |
| F | .33 | .0058 | - - - - | - - - - |
| Isolated tails[a] | | | | |

[a]No corrections applied because of small size of tails.

NATIONAL ADVISORY
COMMITTEE FOR AERONAUTICS

TABLE II

INDEX TO DATA FIGURES

| Model configuration | Tail position number | $\frac{l_t}{b/2}$ | $\frac{h_t}{b/2}$ | Figure number |
|---|---|---|---|---|
| Force-test data | | | | |
| A, with and without tail | 1 | 1.0 | 0.18 | 12(a) |
| | 2 | 1.5 | .18 | 12(b) |
| B, with and without tail | 1 | 1.6 | .29 | 13(a) |
| | 2 | 2.4 | .29 | 13(b) |
| C, with and without tail | 1 | 1.5 | .29 | 14(a) |
| | 2 | 1.5 | .03 | 14(b) |
| | 3 | 2.3 | .29 | 14(c) |
| | 4 | 2.3 | .03 | 14(d) |
| D, with and without tail | 1 | 1.36 | .43 | 15(a) |
| | 2 | 1.36 | .21 | 15(b) |
| | 3 | 1.36 | .03 | 15(c) |
| | 4 | 1.91 | .43 | 15(d) |
| | 5 | 1.91 | .22 | 15(e) |
| | 6 | 1.91 | .04 | 15(f) |
| D, wing alone, with and without high-lift devices | - - - | - - - | - - - | 16 |
| E | - - - | - - - | - - - | 17 |
| F | - - - | - - - | - - - | 18 |
| Isolated tails | - - - | - - - | - - - | 19 |
| Tuft-survey data | | | | |
| B, C, without tail | - - - | 1.5,2.3 | - - - | 20 |
| D, wing alone | - - - | 1.36,1.91 | - - - | 21 |
| D, wing alone, equipped with flap and slat | - - - | 1.91 | - - - | 22 |
| E | - - - | 1.36,2.03 | - - - | 23 |
| F | - - - | 1.25,1.86 | - - - | 24 |
| Analysis plots | | | | |
| Comparison of force and tuft data | | | | 25 and 26 |
| Effect of aspect ratio | | | | 27 |
| Effect of taper ratio | | | | 28 |
| Effect of tail span | | | | 29 |
| Comparison of measured and computed values of $d\epsilon'/d\alpha$ | | | | 30 |

NATIONAL ADVISORY
COMMITTEE FOR AERONAUTICS

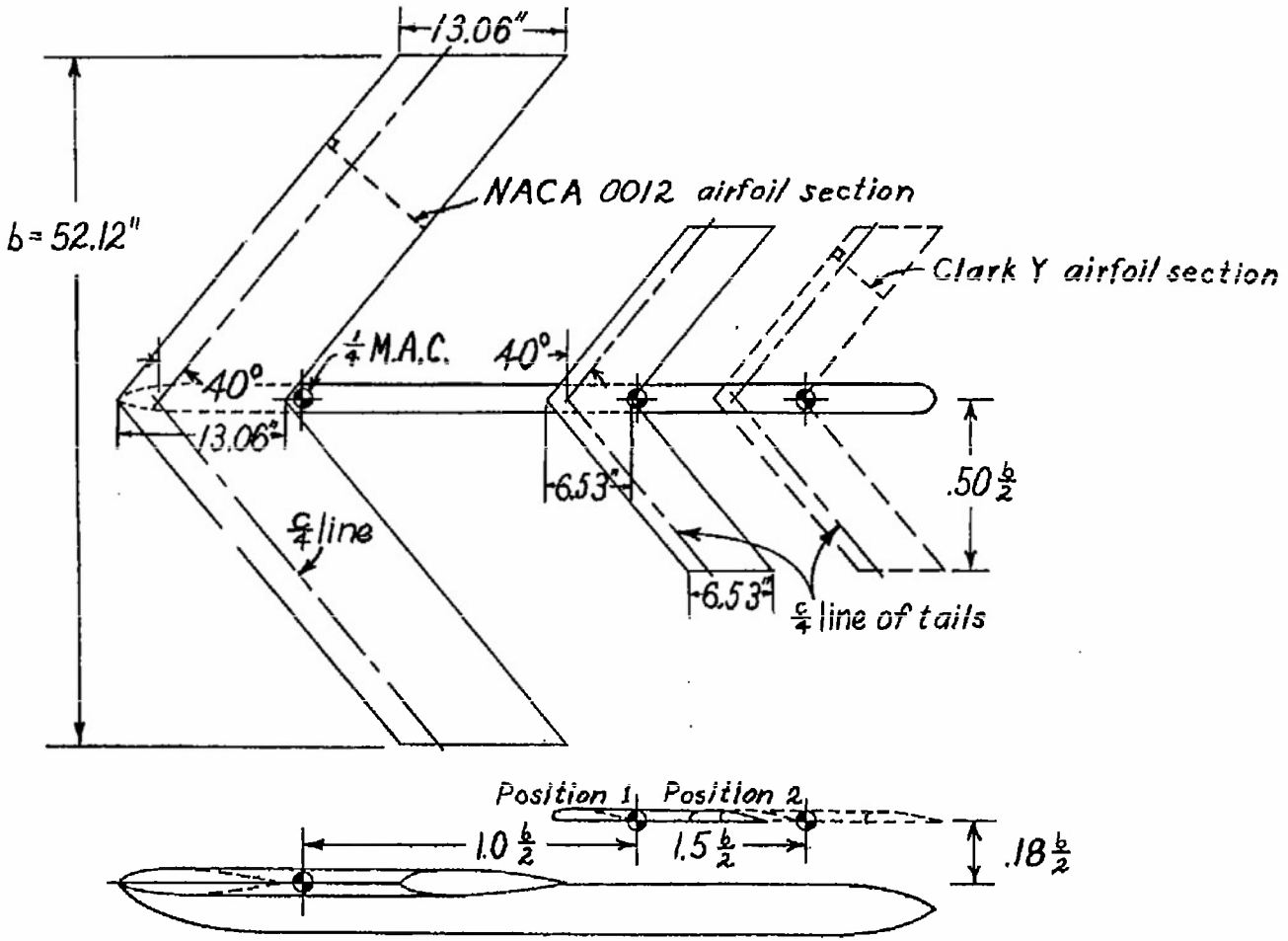


NATIONAL ADVISORY
COMMITTEE FOR AERONAUTICS

Figure 1.- Details of model A showing wing-tail combinations tested. Wing: $\frac{c_R}{c_T} = 1.0$; $A = 4.0$; $\Lambda_{c/4} = 40^\circ$. Tail: $\frac{c_R}{c_T} = 1.0$; $A_t = 4.0$; $\Lambda_{c/4} = 40^\circ$.

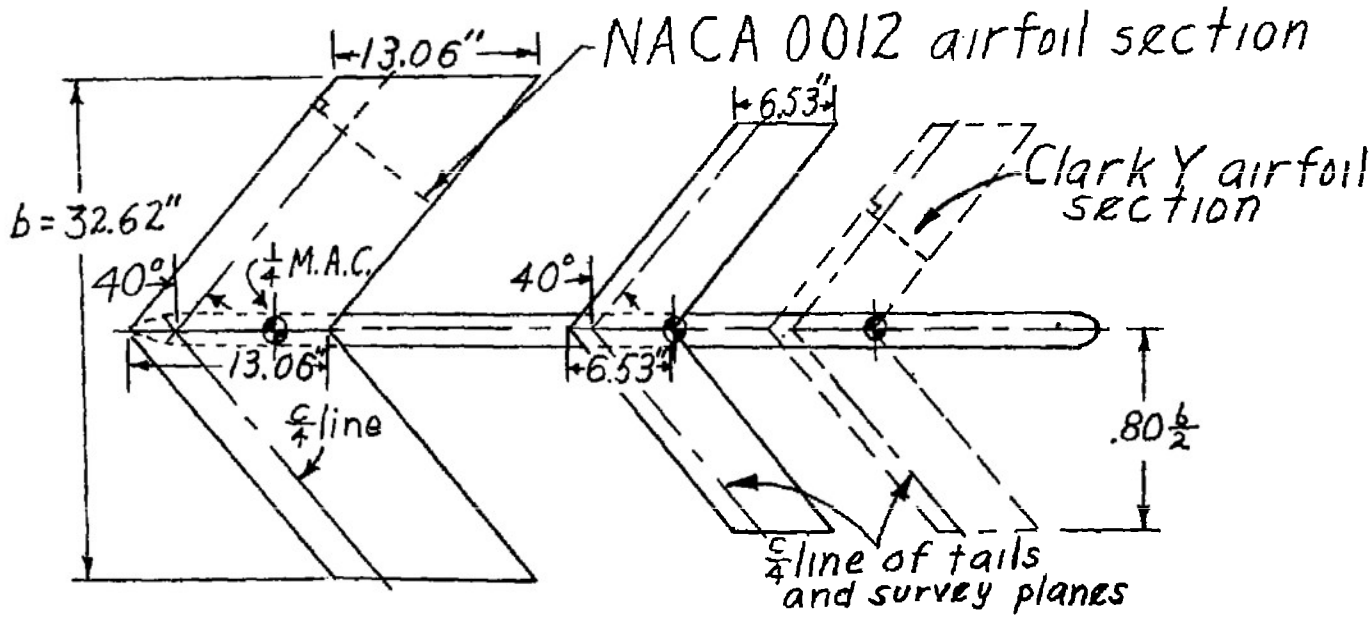


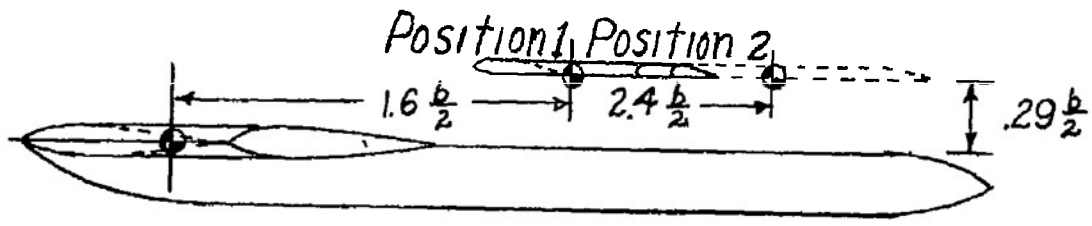


NATIONAL ADVISORY COMMITTEE FOR AERONAUTICS

Figure 2.- Details of model B showing wing-tail combinations tested. Wing: $\frac{c_R}{c_T} = 1.0$; $A = 2.5$; $\Lambda_{c/4} = 40^\circ$. Tail: $\frac{c_R}{c_T} = 1.0$; $A_t = 4.0$; $\Lambda_{c/4} = 40^\circ$.

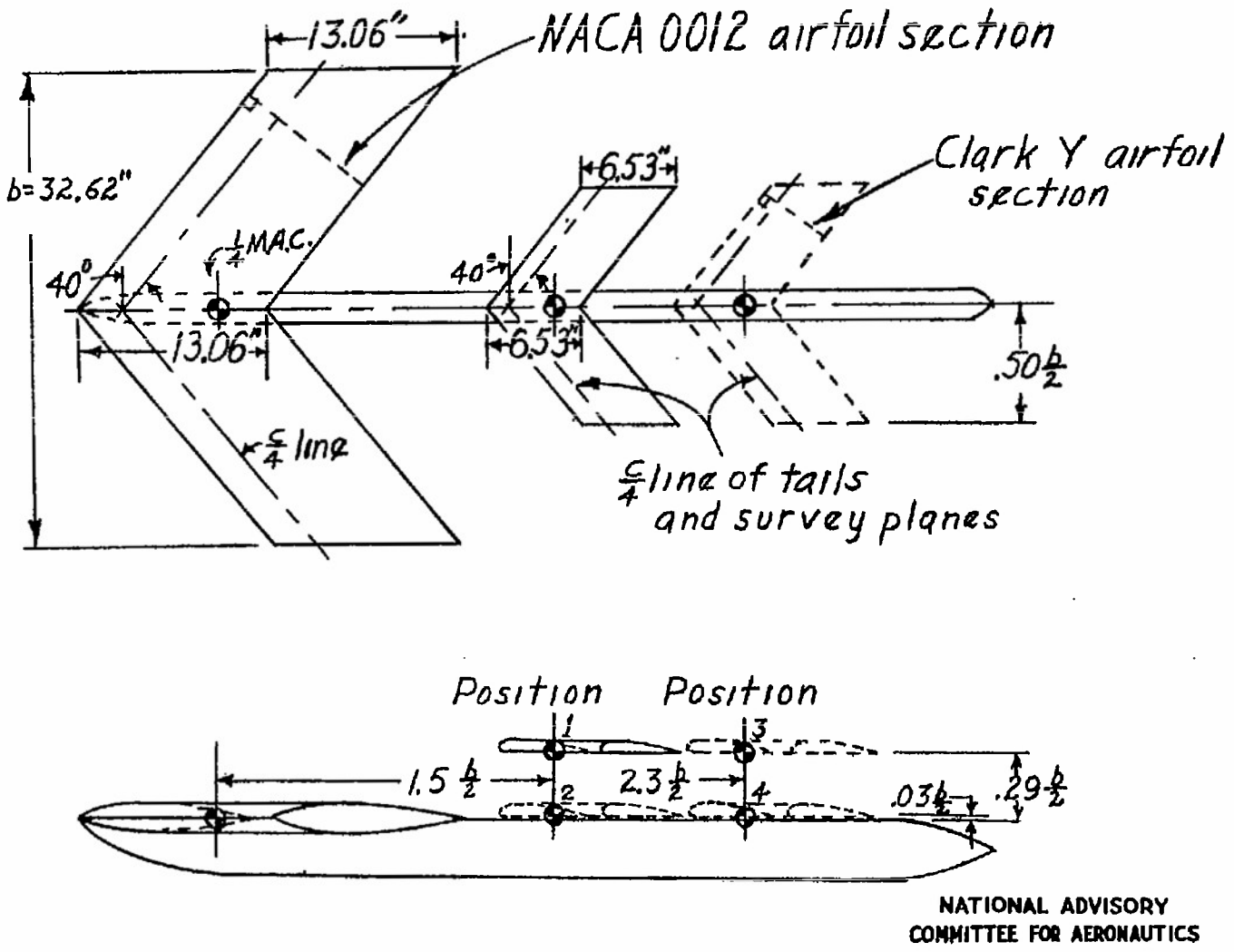


NATIONAL ADVISORY COMMITTEE FOR AERONAUTICS

Figure 3.- Details of model C showing wing-tail combinations tested. Wing: $\frac{c_R}{c_T} = 1.0$; $A = 2.5$; $\Lambda_{c/4} = 40^\circ$. Tail: $\frac{c_R}{c_T} = 1.0$; $A_t = 2.5$; $\Lambda_{c/4} = 40^\circ$.

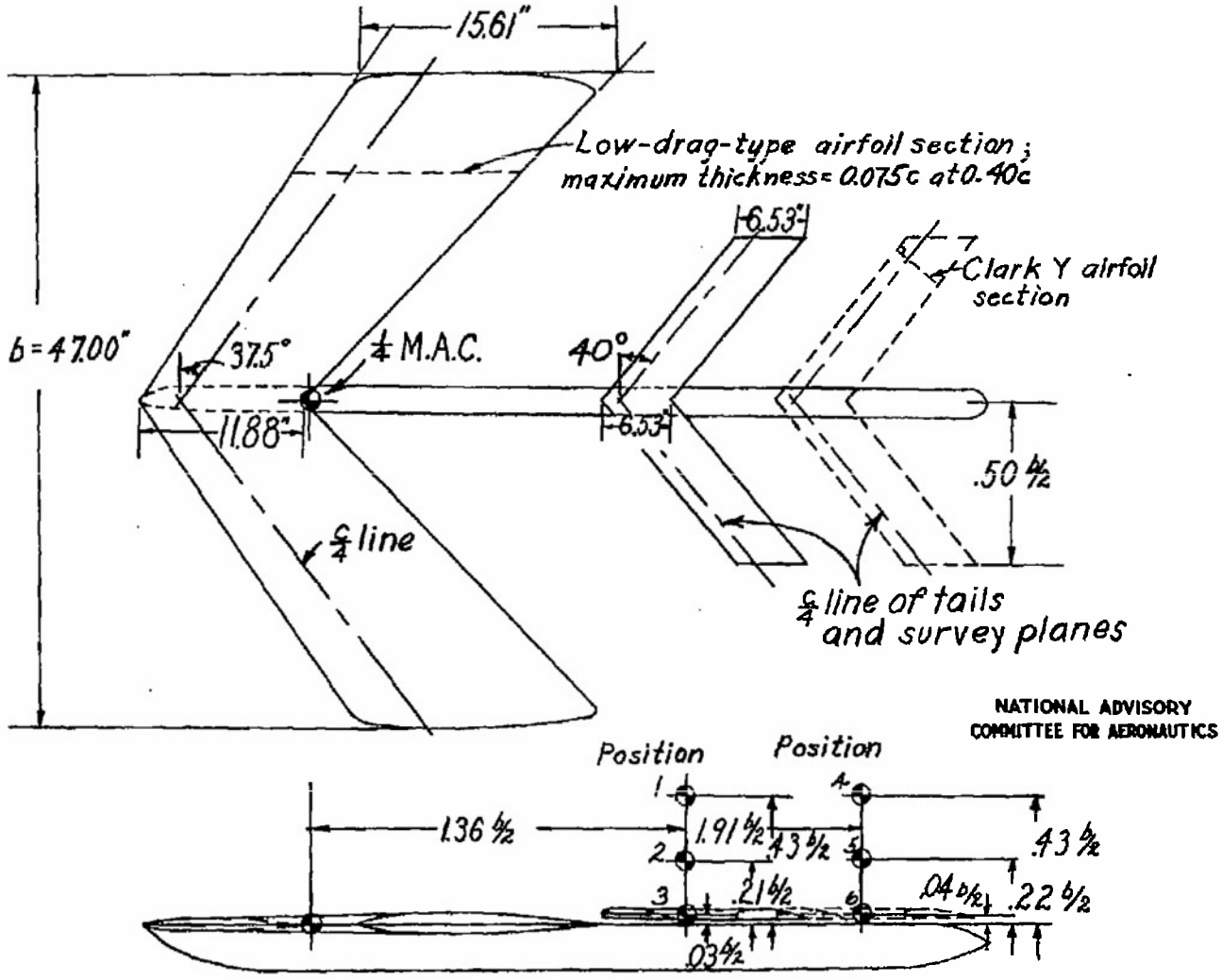


Figure 4.- Details of model D showing wing-tail combinations tested. Wing: $\frac{c_R}{c_T} = 0.617$; $A = 3.0$; $\Lambda_{c/4} = 37.5^\circ$. Tail: $\frac{c_R}{c_T} = 1.0$; $A_t = 3.6$; $\Lambda_{c/4} = 40^\circ$.

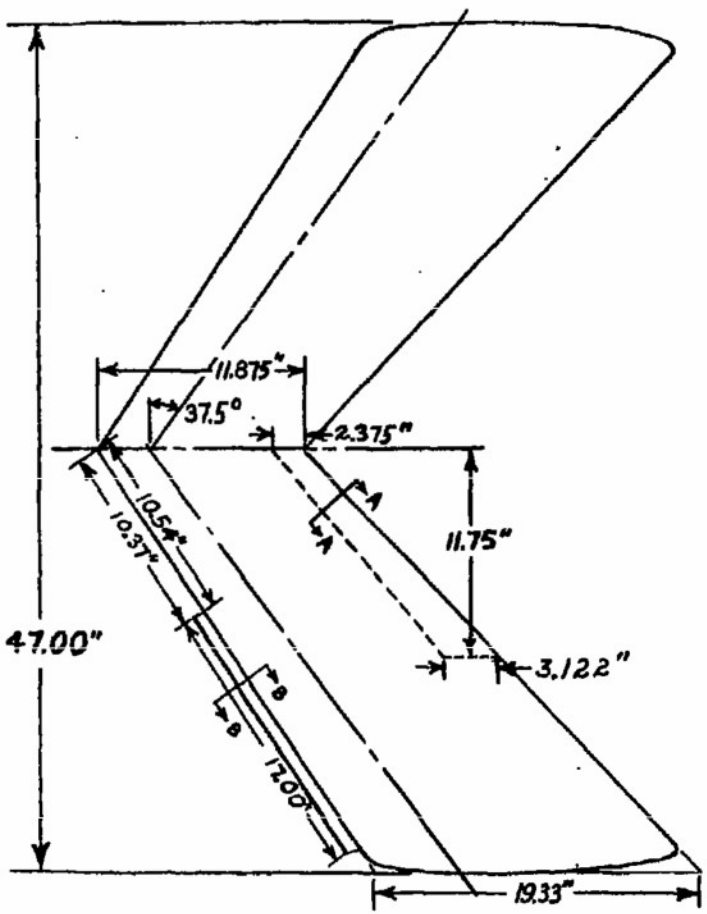


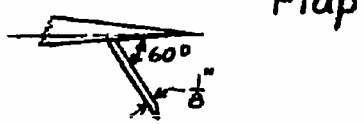


Section A-A

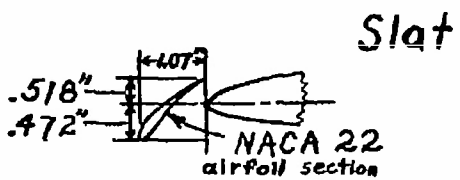


Section B-B

ORDINATES FOR NACA 22 AIRFOIL
[Stations and ordinates in percent of wing chord]

| Station | Upper surface | Lower surface |
|---|---|---|
| 0 | 2.88 | 2.88 |
| 1.25 | 5.40 | 1.09 |
| 2.5 | 6.48 | .65 |
| 5.0 | 8.02 | .28 |
| 7.5 | 9.11 | .08 |
| 10 | 9.96 | 0 |
| 20 | 12.29 | .44 |
| 30 | 13.35 | 1.46 |
| 40 | 13.42 | 3.08 |
| 50 | 12.60 | 4.78 |
| 60 | 11.12 | 5.63 |
| 70 | 9.15 | 5.79 |
| 80 | 6.68 | 4.68 |
| 90 | 3.95 | 2.67 |
| 100 | 1.13 | 0 |

NATIONAL ADVISORY
COMMITTEE FOR AERONAUTICS

Figure 5.- Details of flap and slat on wing of model D.

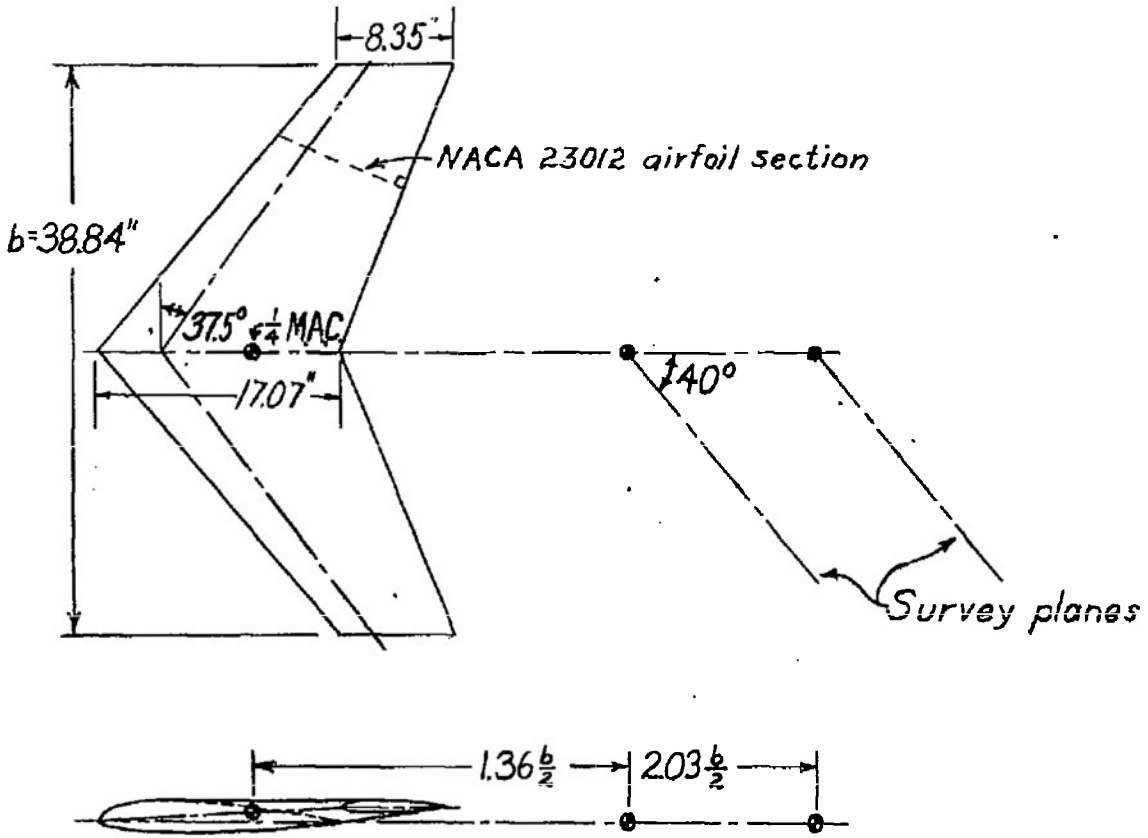


NATIONAL ADVISORY
COMMITTEE FOR AERONAUTICS

Figure 6.- Details of model E showing tuft-survey planes. $\frac{c_R}{c_T} = 2.04$; $A = 3$; $\Lambda_{c/4} = 37.5^{\circ}$.

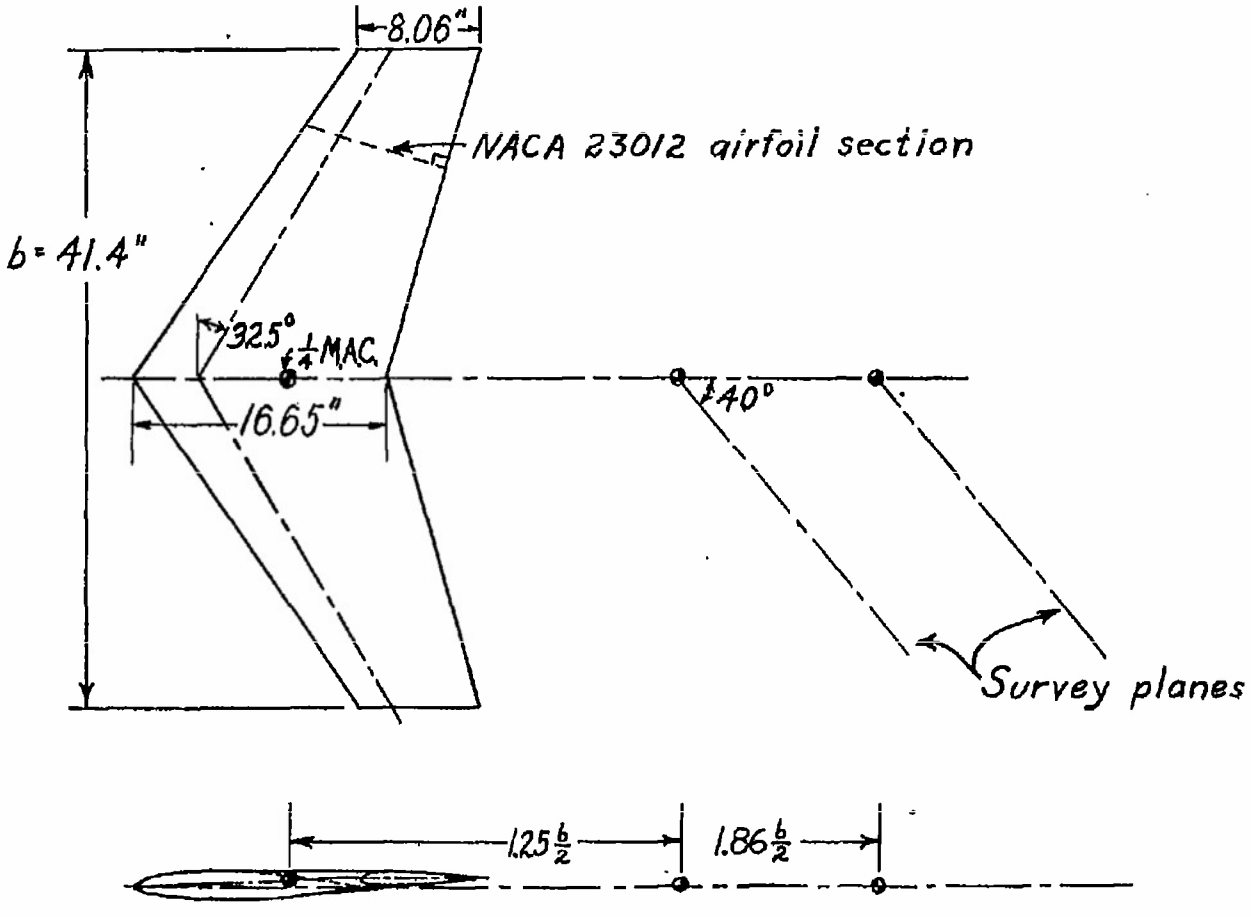


NATIONAL ADVISORY
COMMITTEE FOR AERONAUTICS

Figure 7.- Details of model F showing tuft-survey planes. $\frac{c_R}{c_T} = 2.06$; $A = 3.3$; $\Lambda_{c/4} = 32.5^{\circ}$.

| Station | Ordinate |
|---|---|
| 0 | 0 |
| 1.08 | .43 |
| 2.16 | .49 |
| 3.22 | .52 |
| 6.45 | .52 |
| 8.75 | 0 |

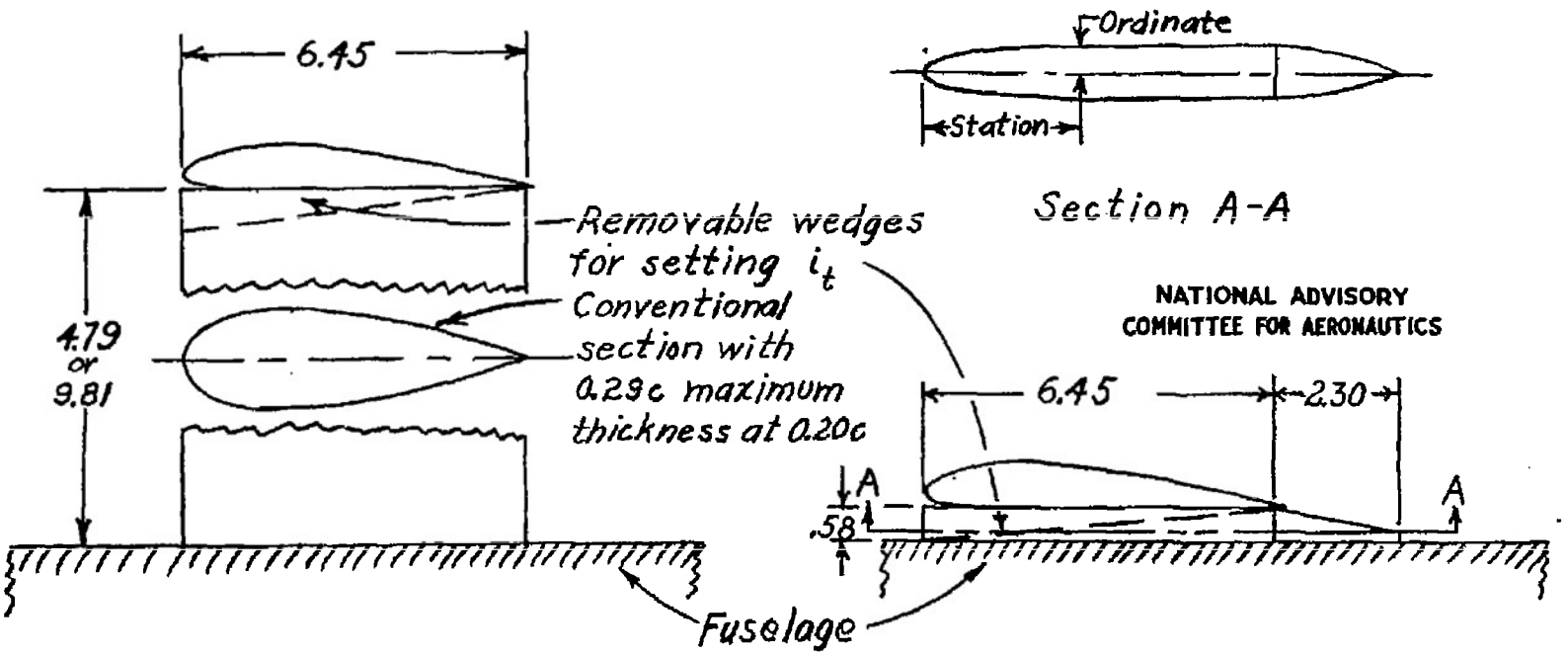


(a) High tail position.

(b) Low tail position.

Figure 8.- Fittings for high and low tail positions on fuselage of models A, B, C, and D. All dimensions in inches except where noted.

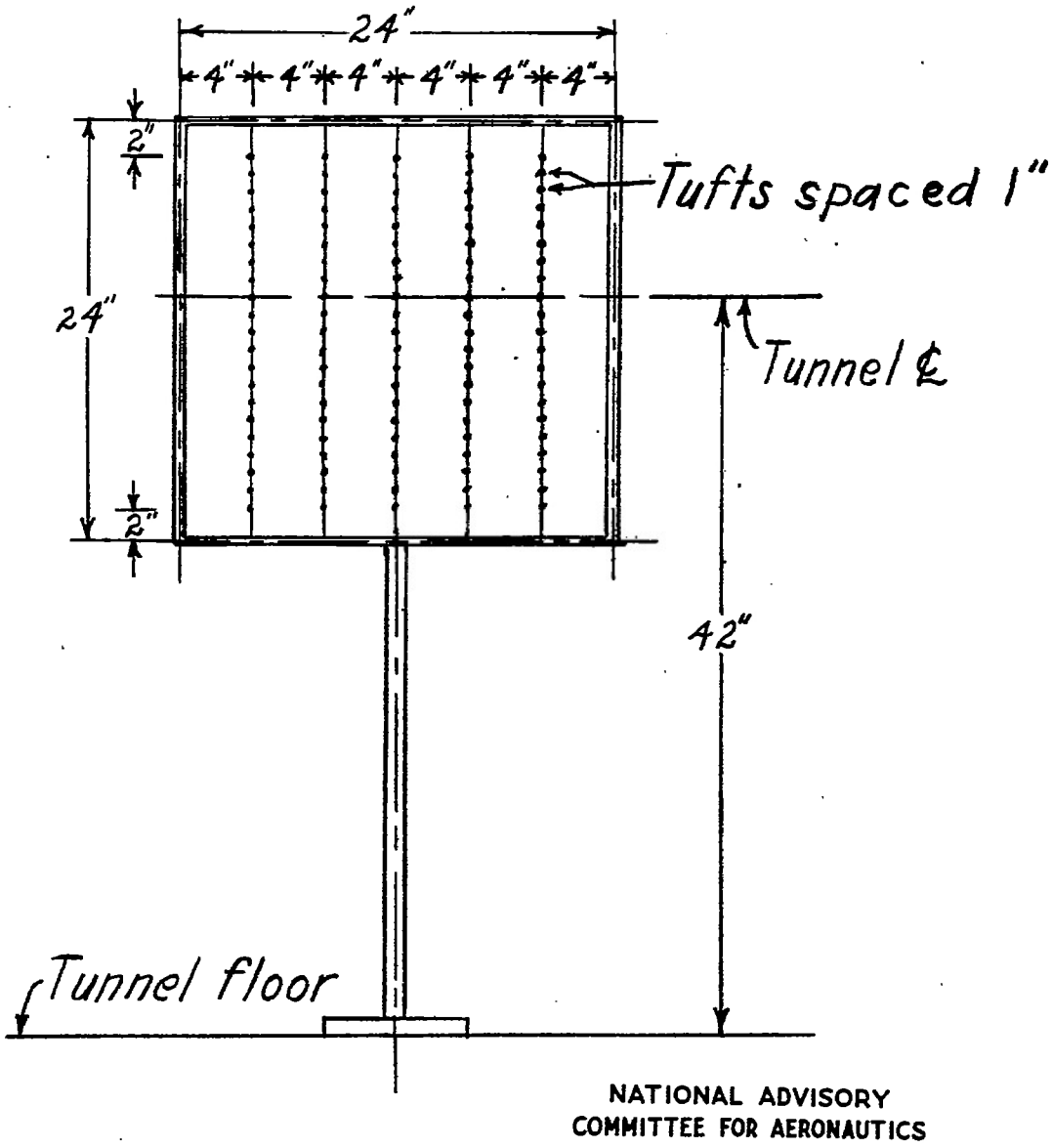


Figure 9.- Survey rig for measuring downwash angles.

Figure 10.- Side view of tuft-survey rig in tunnel during test run.

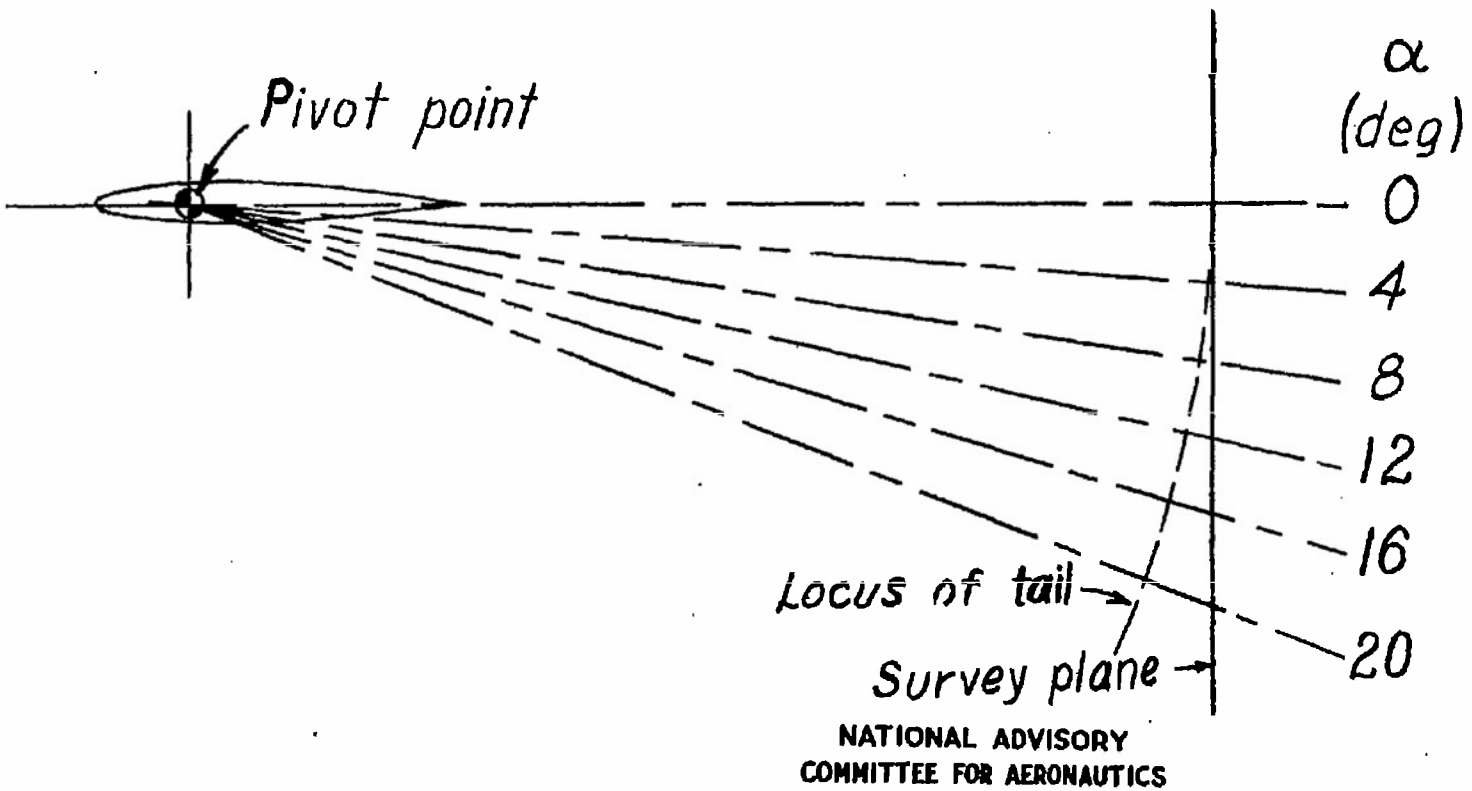


Figure 11.- Location of survey plane with respect to model at various angles of attack.

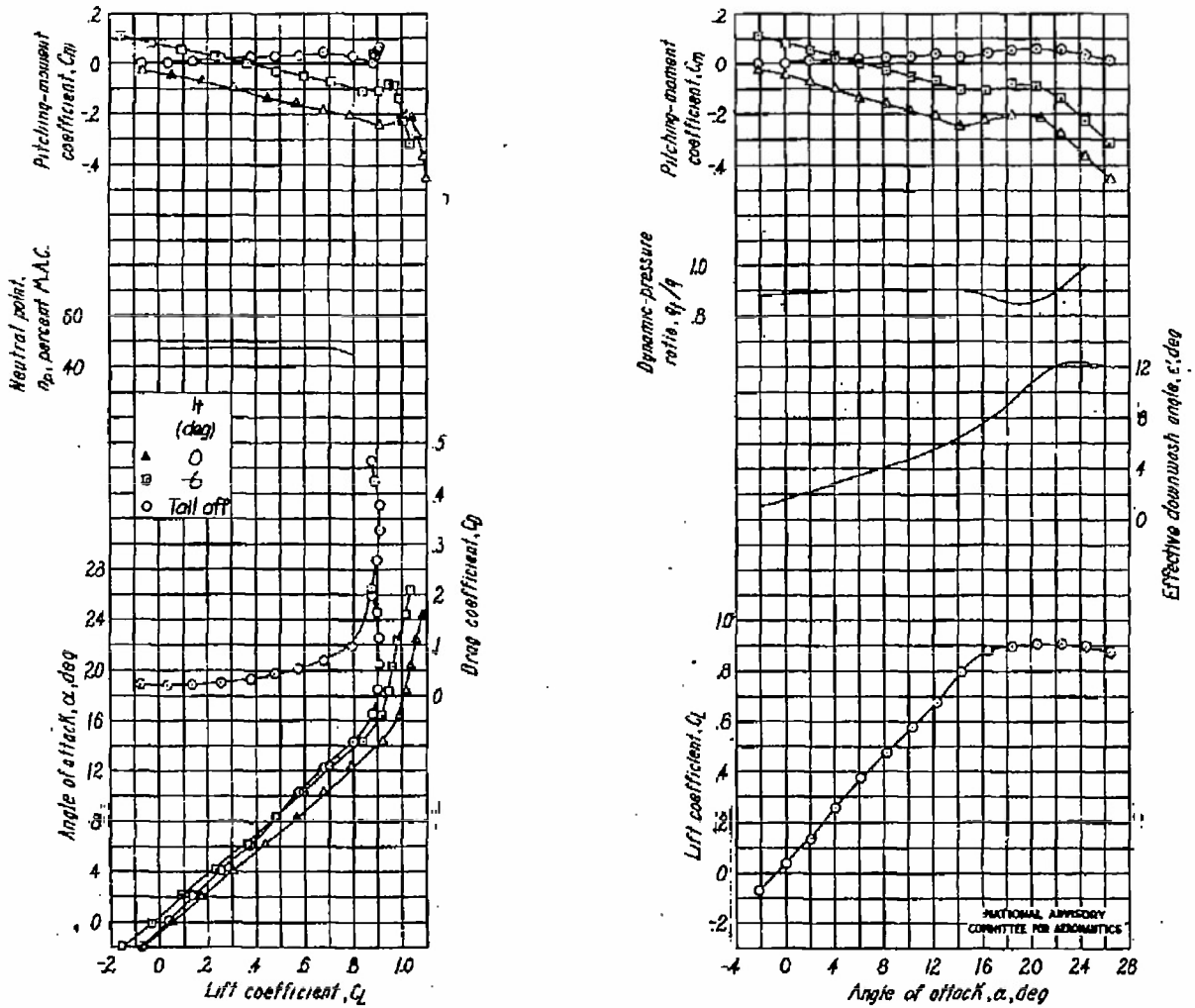


(a) Position 1.

Figure 12.- Effect of horizontal tail setting and position on aerodynamic characteristics of model A. Wing: $\frac{c_R}{c_T} = 1.0$; $A = 4.0$; $\Lambda_{c/4} = 40^\circ$. Tail: $\frac{c_R}{c_T} = 1.0$; $A_t = 4.0$; $\Lambda_{c/4} = 40^\circ$.

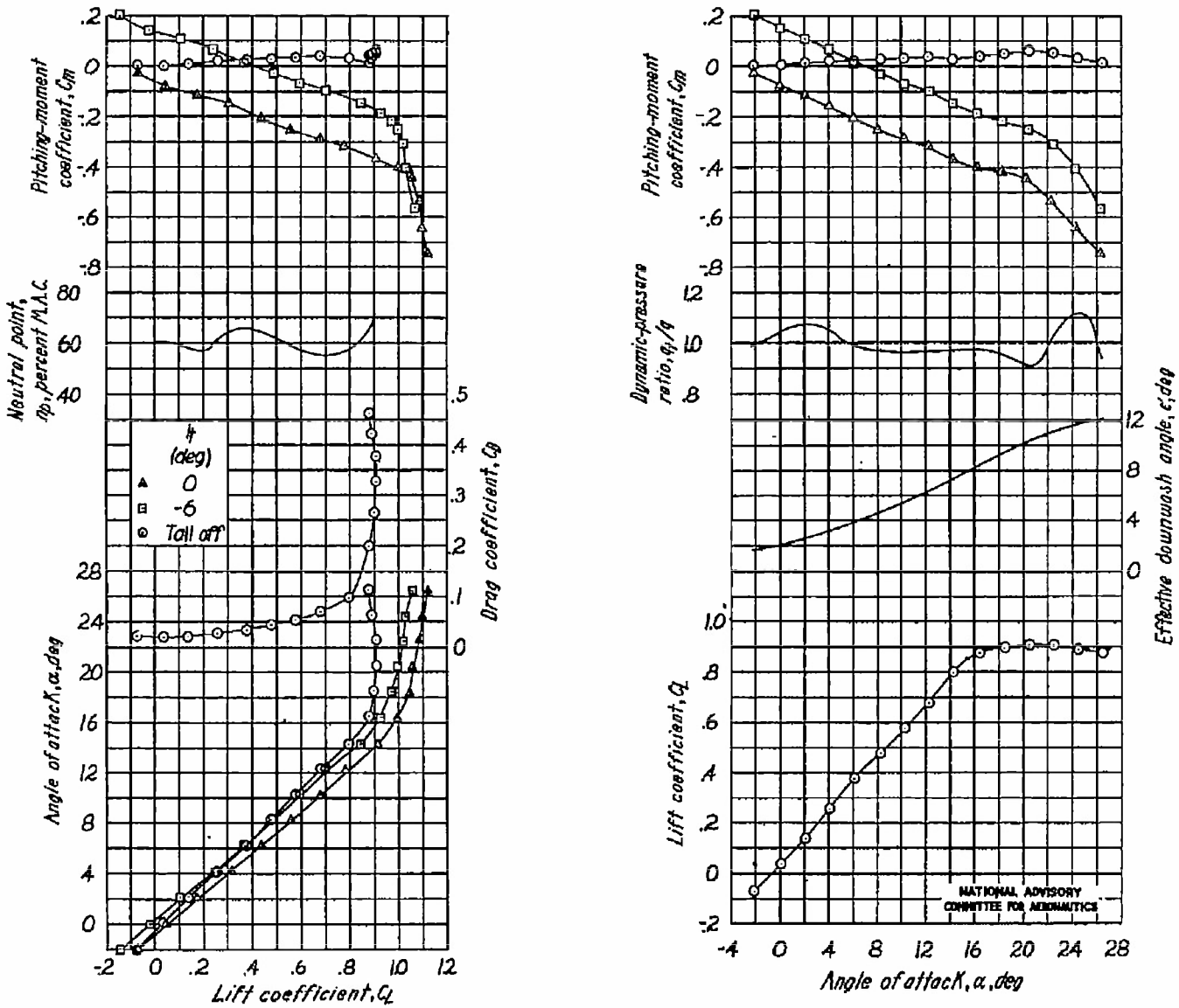


(b) Position 2.

Figure 12.- Concluded.

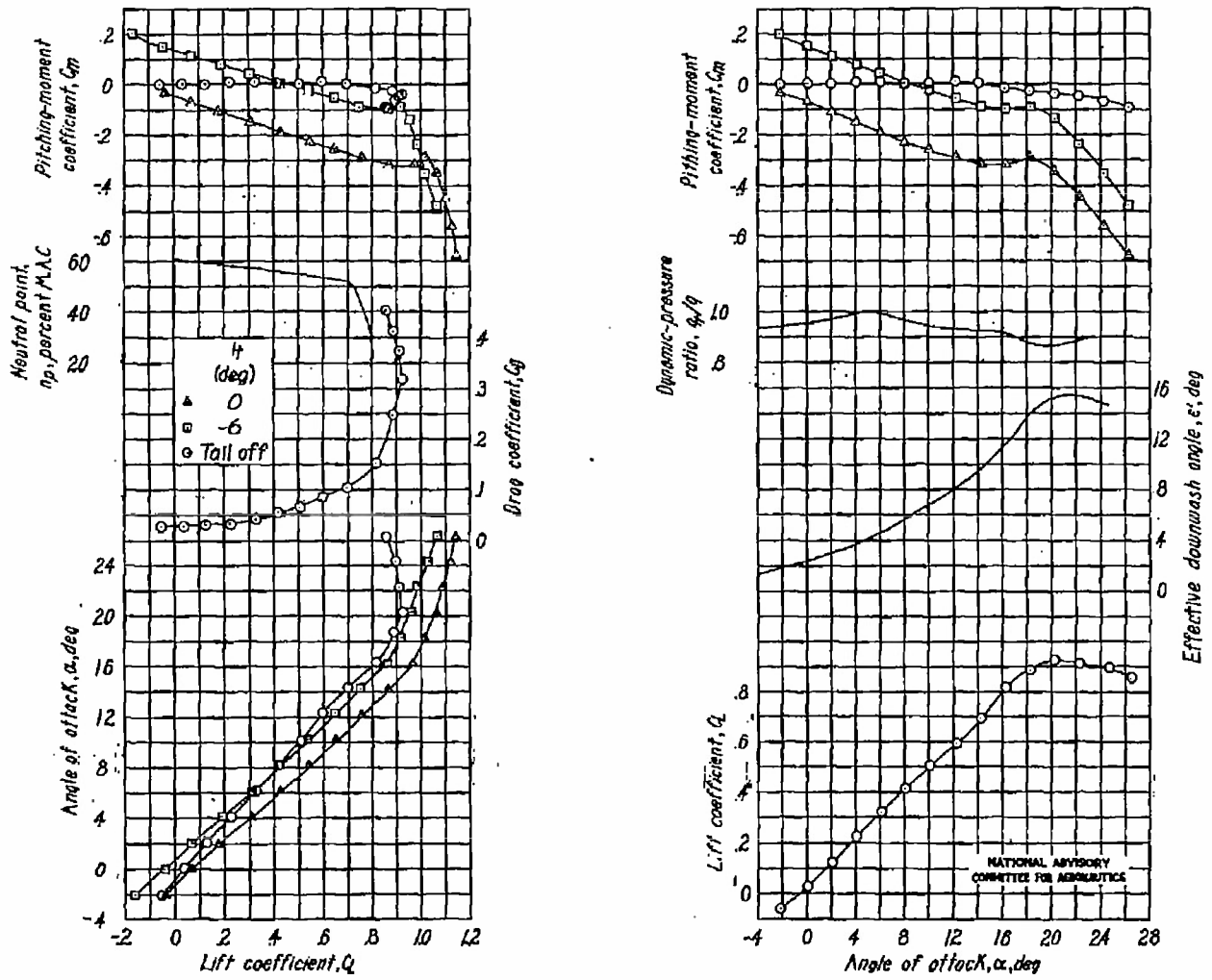


(a) Position 1.

Figure 13.- Effect of horizontal tail setting and position on aerodynamic characteristics of model B. Wing: $\frac{c_R}{c_T} = 1.0$; $A = 2.5$; $\Lambda_{c/4} = 40^\circ$. Tail: $\frac{c_R}{c_T} = 1.0$; $A_t = 4.0$; $\Lambda_{c/4} = 40^\circ$.

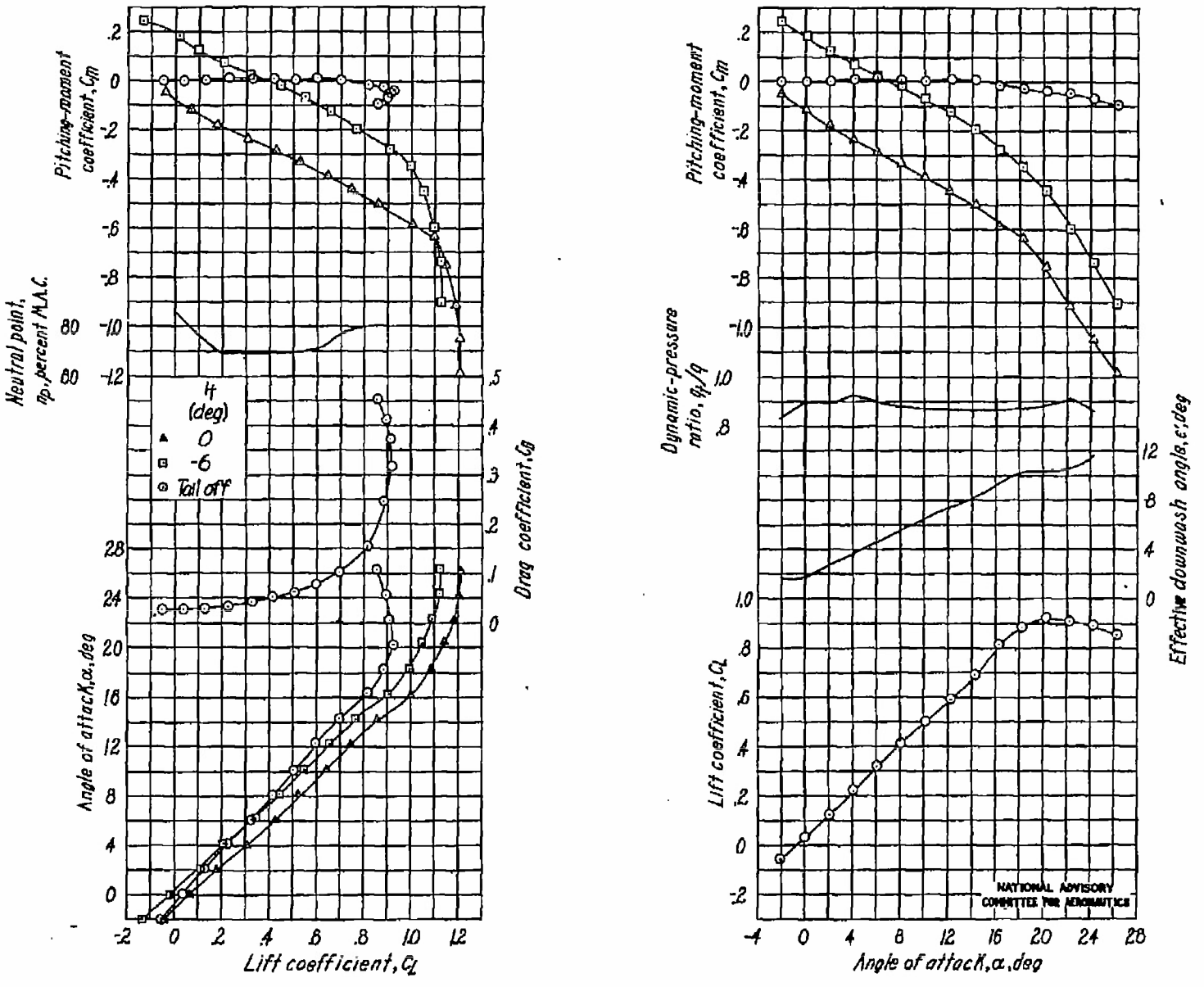


(b) Position 2.

Figure 13.- Concluded.

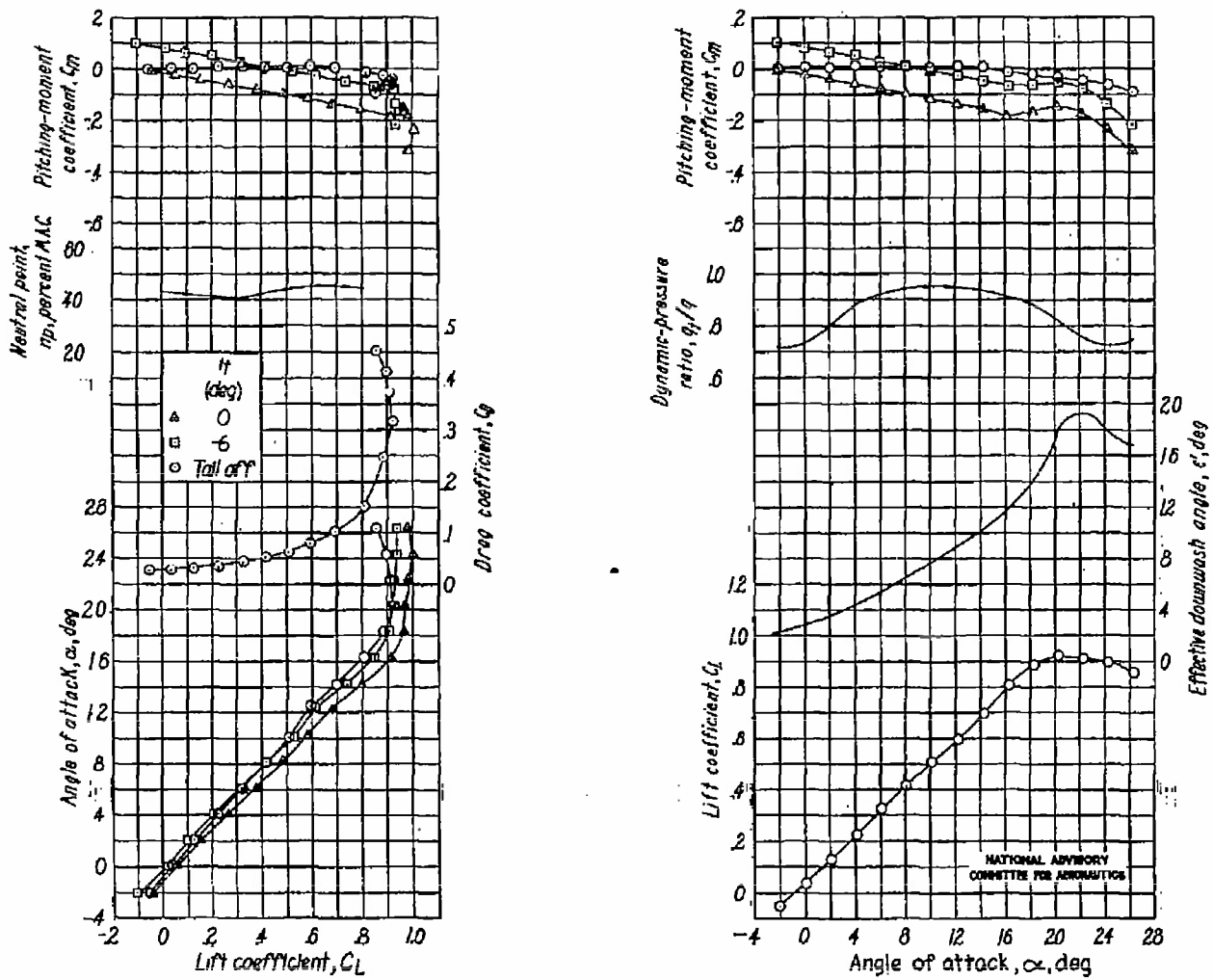


(a) Position 1.

Figure 14.- Effect of horizontal tail setting and position on aerodynamic characteristics of model C. Wing: $\frac{c_R}{c_T} = 1.0$; $A = 2.5$; $\Lambda_{c/4} = 40^\circ$. Tail: $\frac{c_R}{c_T} = 1.0$; $A_t = 2.5$; $\Lambda_{c/4} = 40^\circ$.

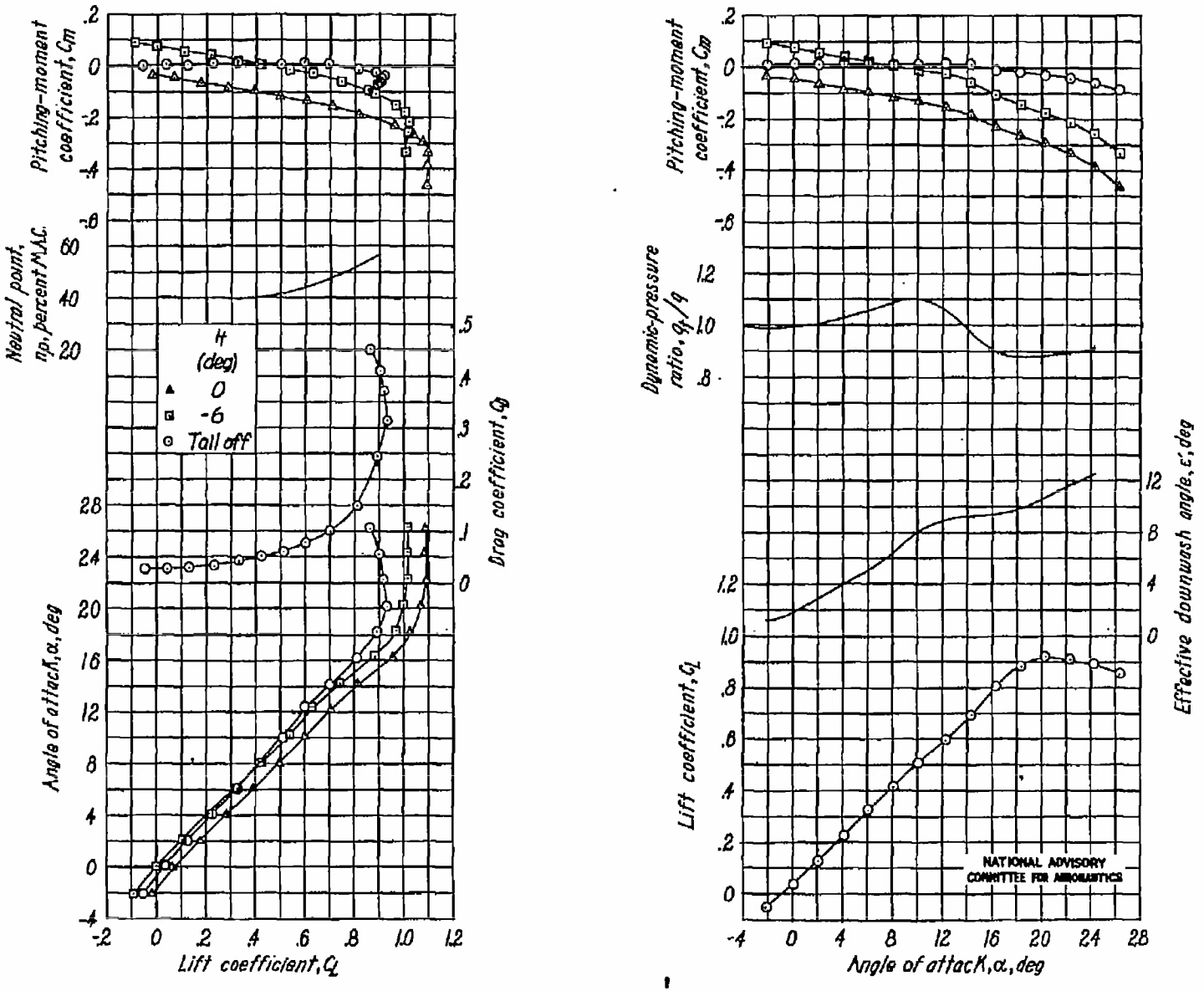


(b) Position 2.

Figure 14.- Continued.

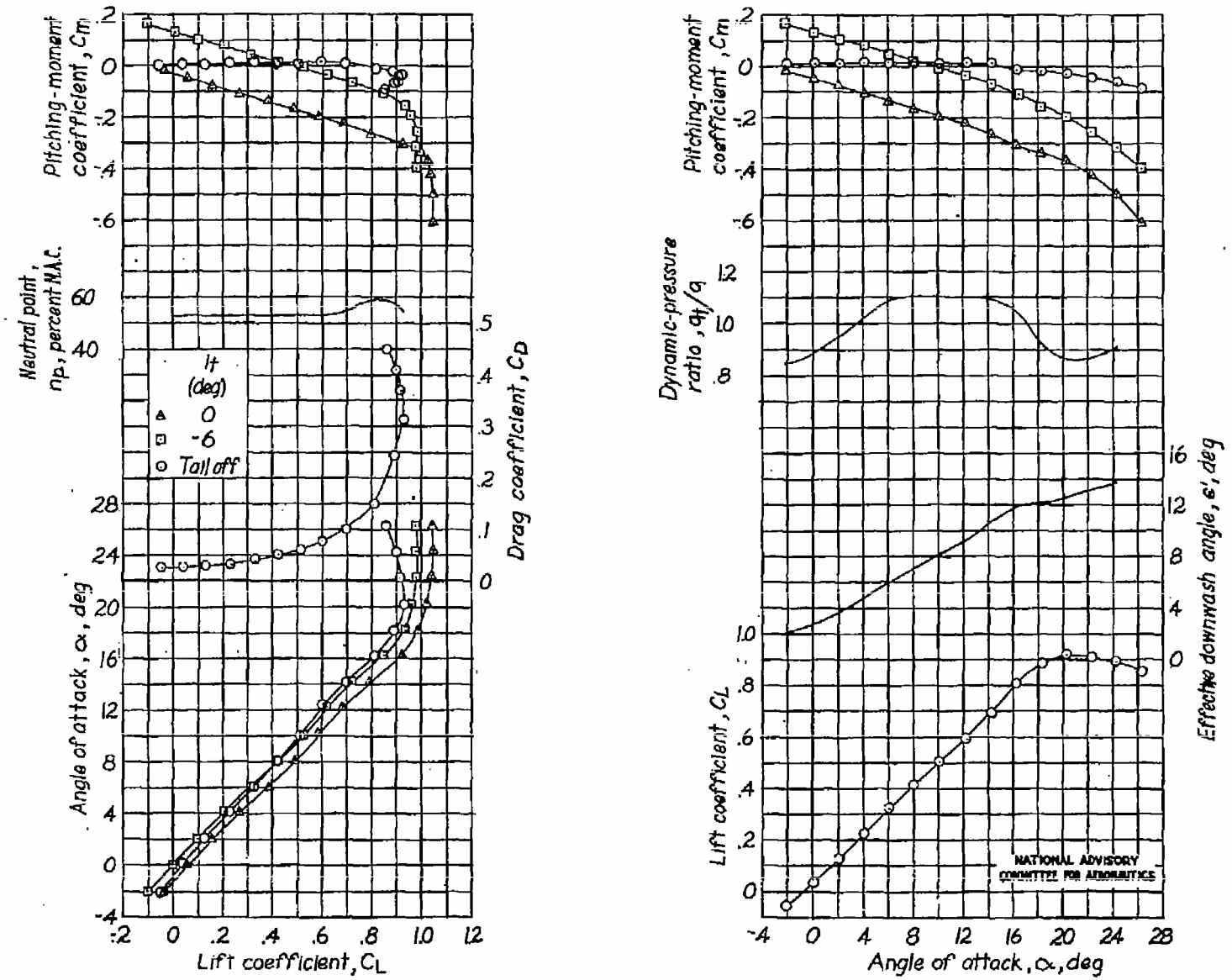


(c) Position 3.

Figure 14.- Continued.

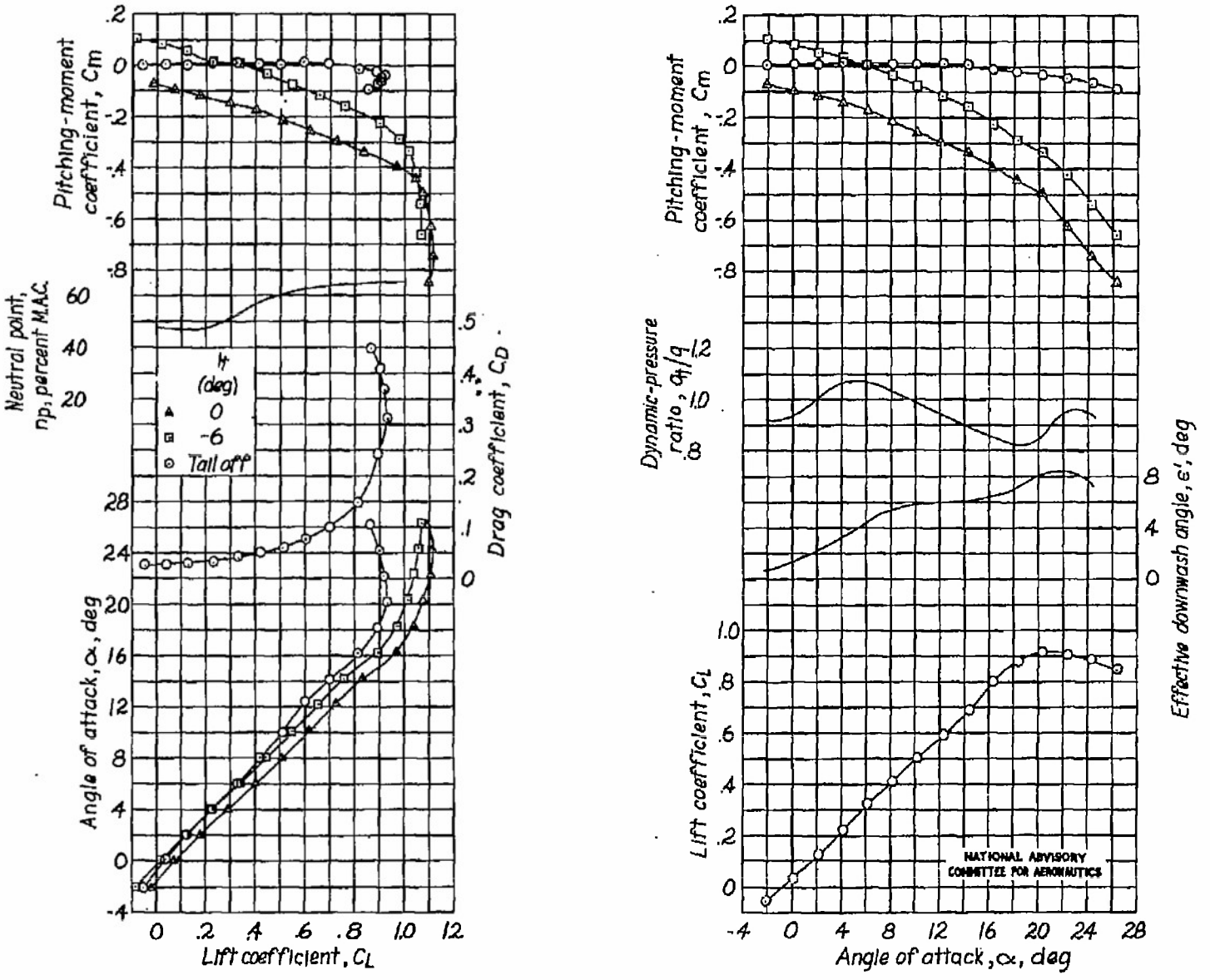


(d) Position 4.

Figure 14.- Concluded.

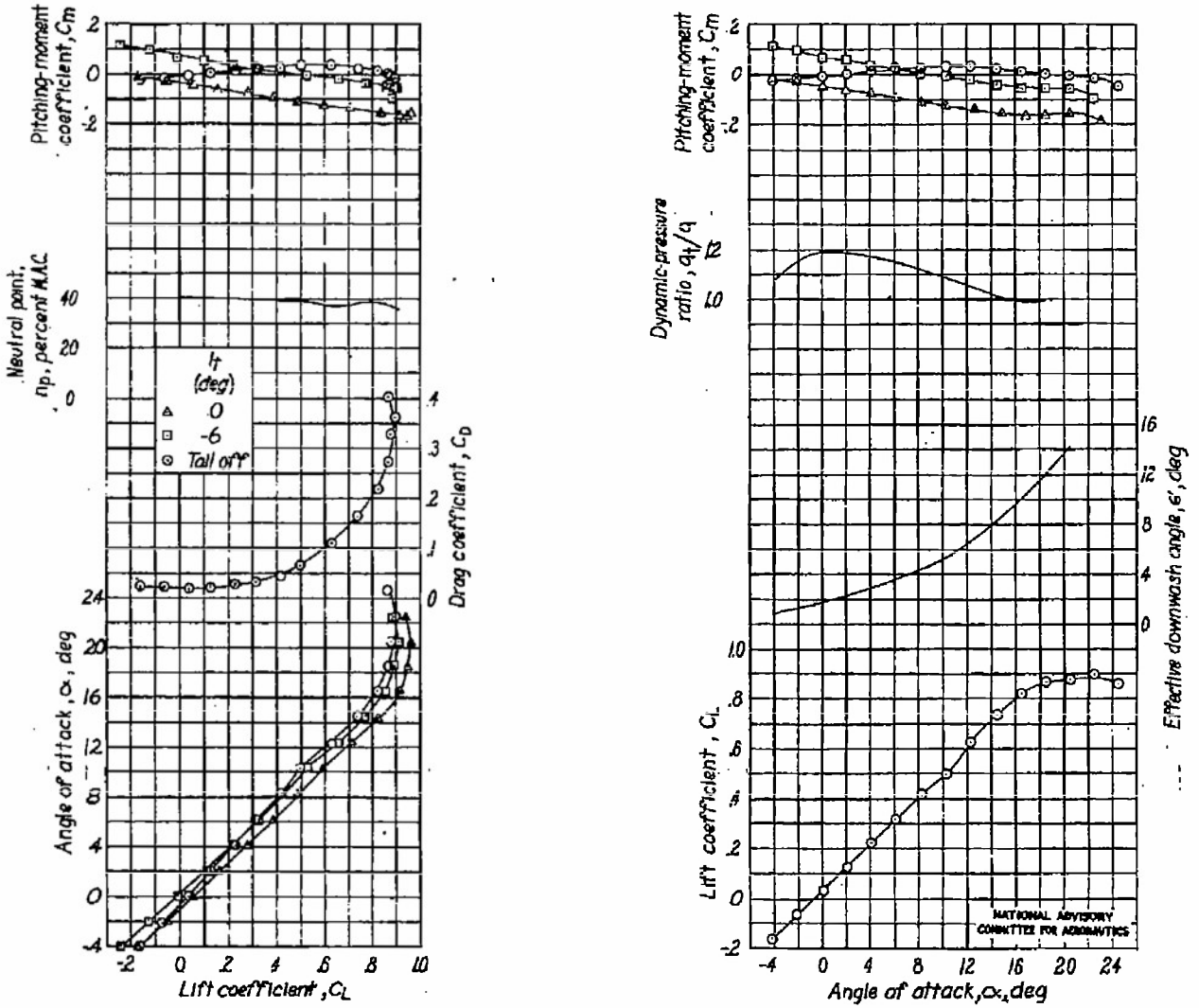


(a) Position 1.

Figure 15.- Effect of horizontal tail setting and position on aerodynamic characteristics of model D. Wing: $\frac{c_R}{c_T} = 0.617$; $A = 3.0$; $\Lambda_{c/4} = 37.5^{\circ}$. Tail: $\frac{c_R}{c_T} = 1.0$; $A_t = 3.6$; $\Lambda_{c/4} = 40^{\circ}$.

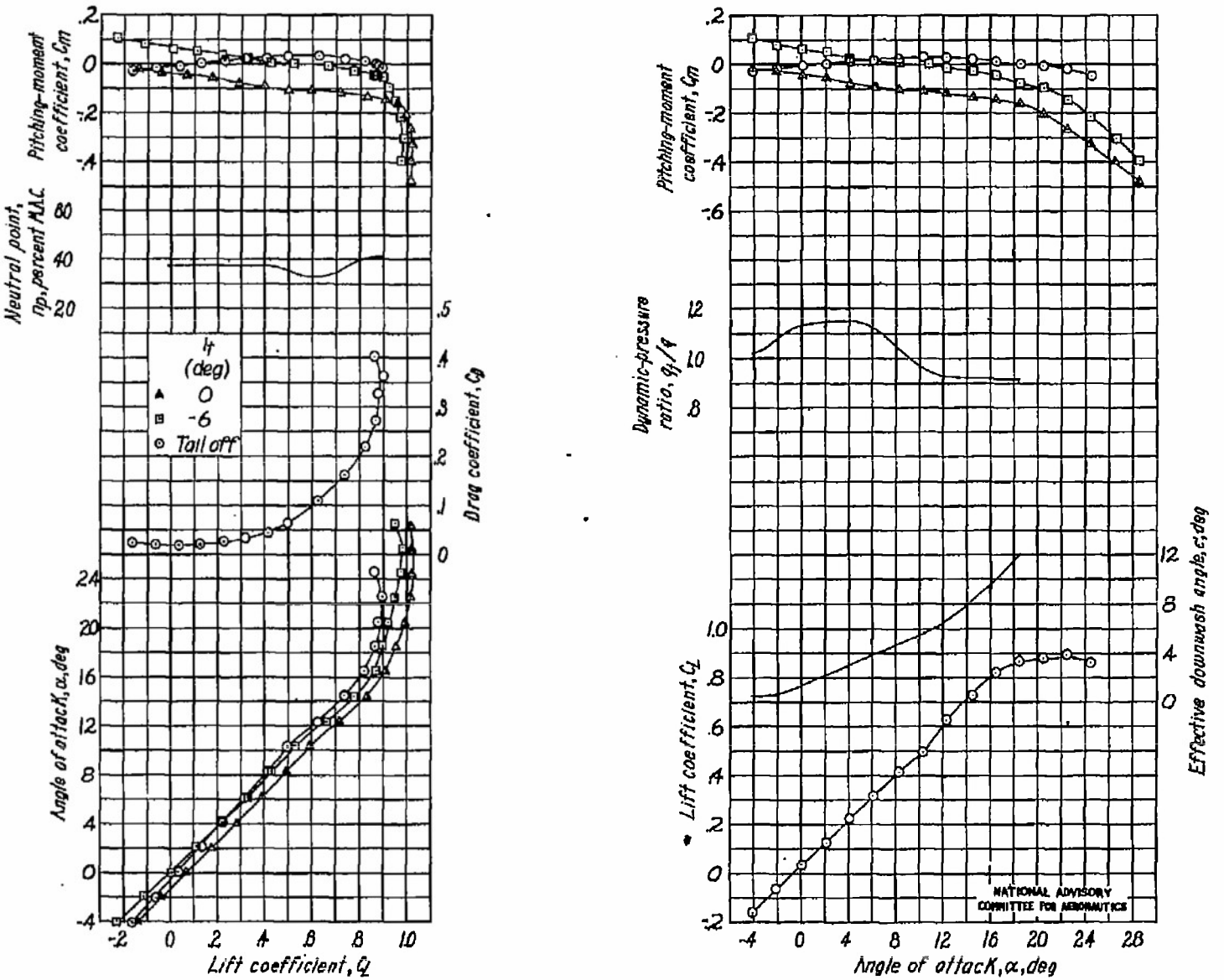


(b) Position 2.

Figure 15.- Continued.

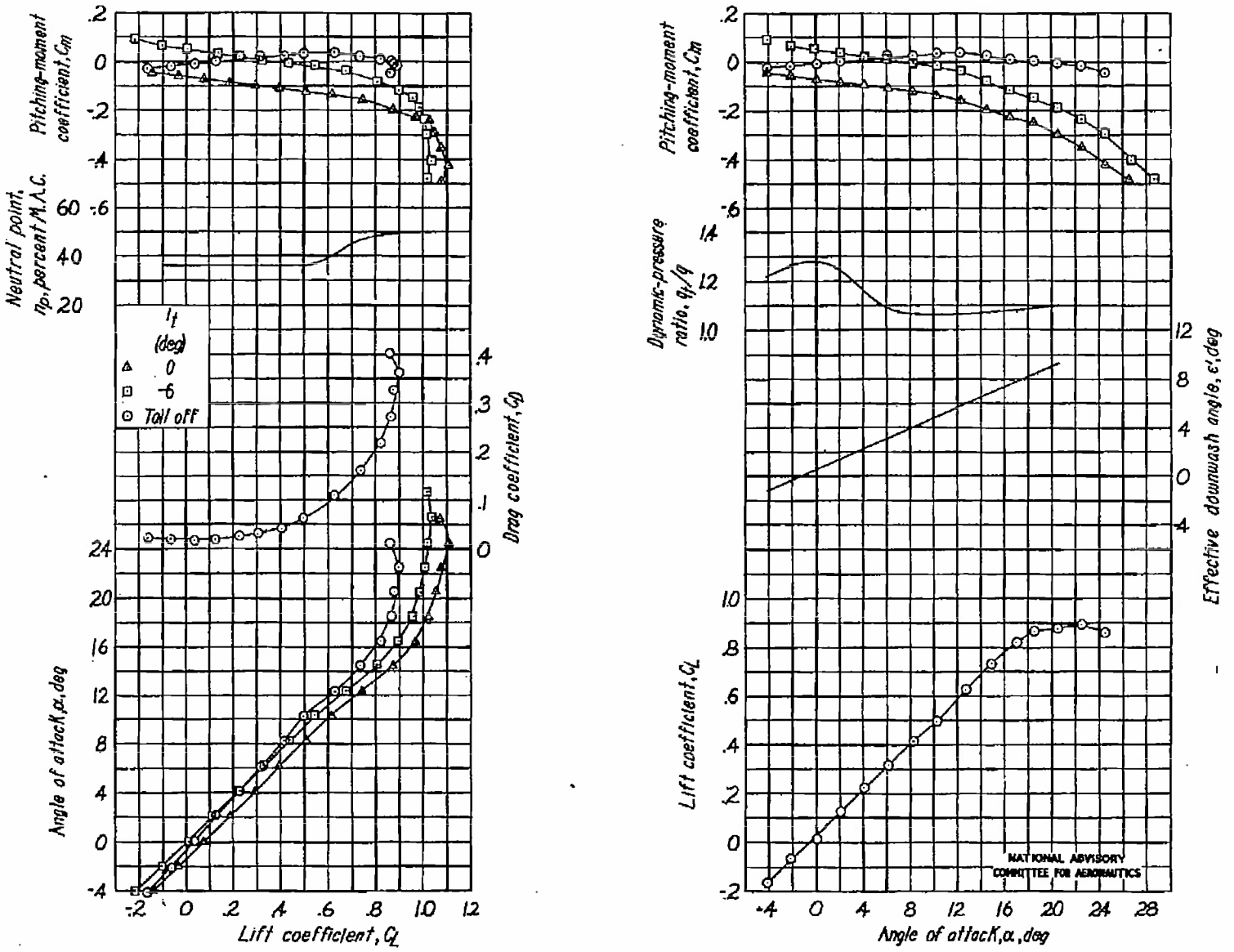


(c) Position 3.

Figure 15.- Continued.

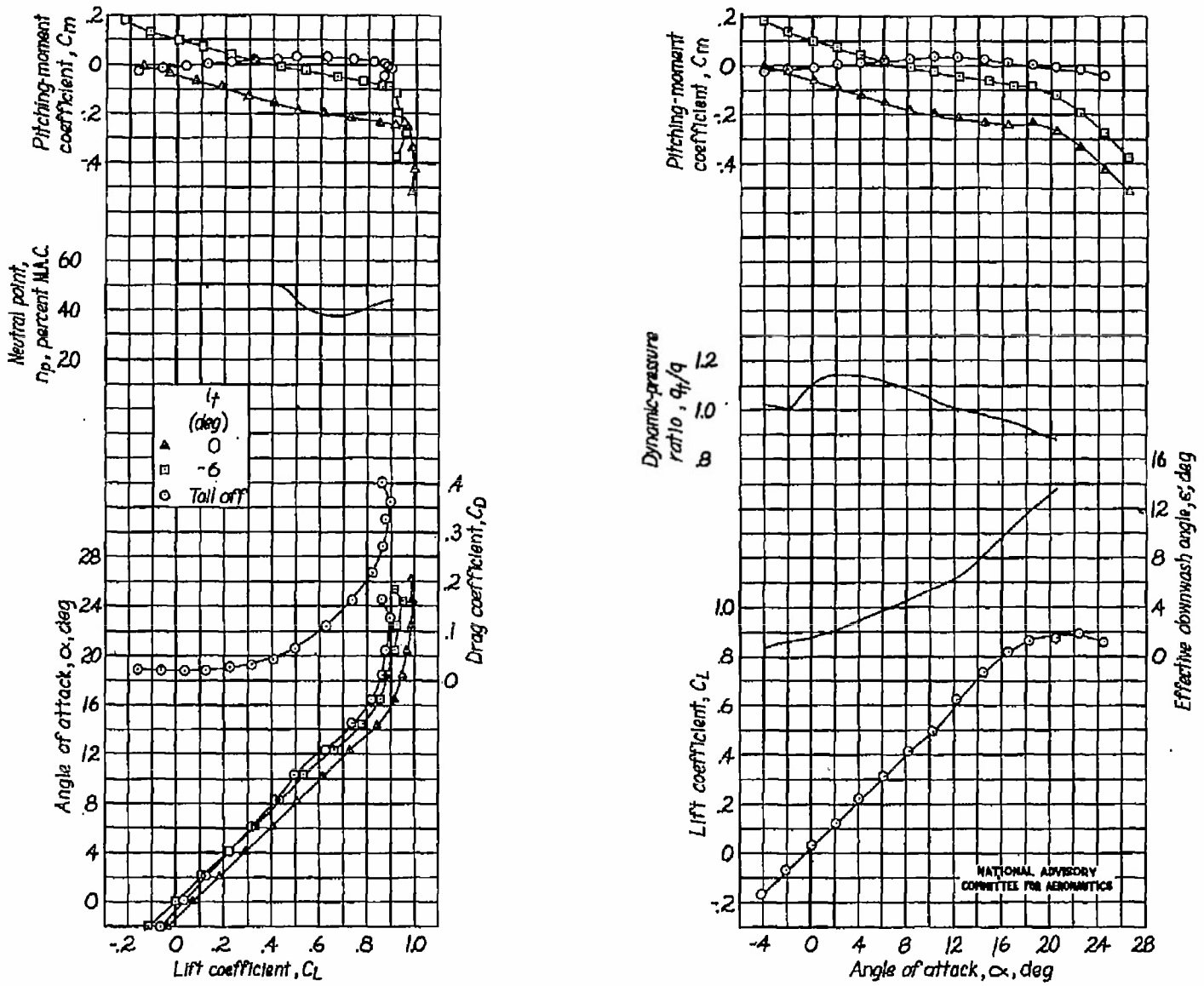


(d) Position 4.

Figure 15.- Continued.

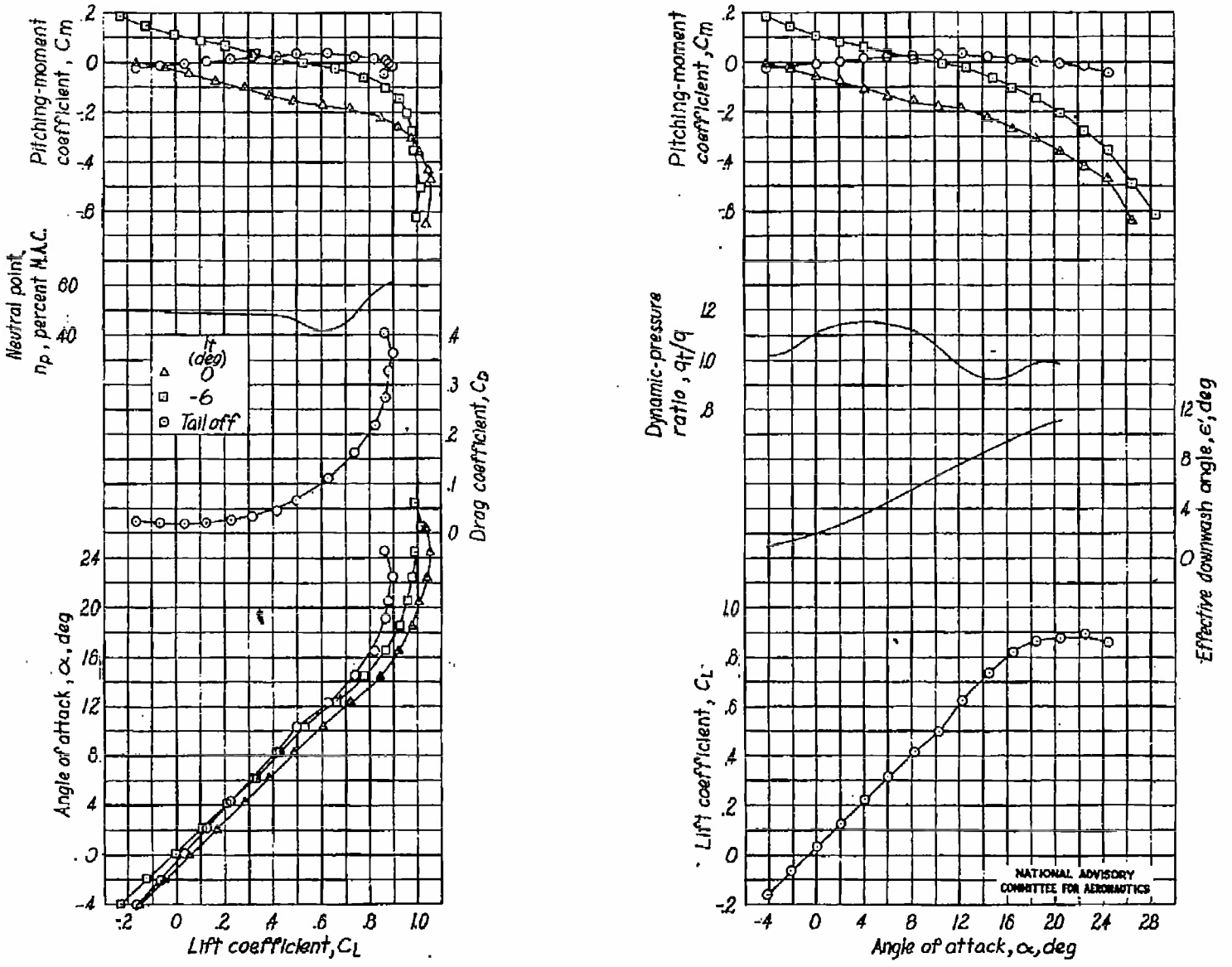


(e) Position 5.

Figure 15.- Continued.

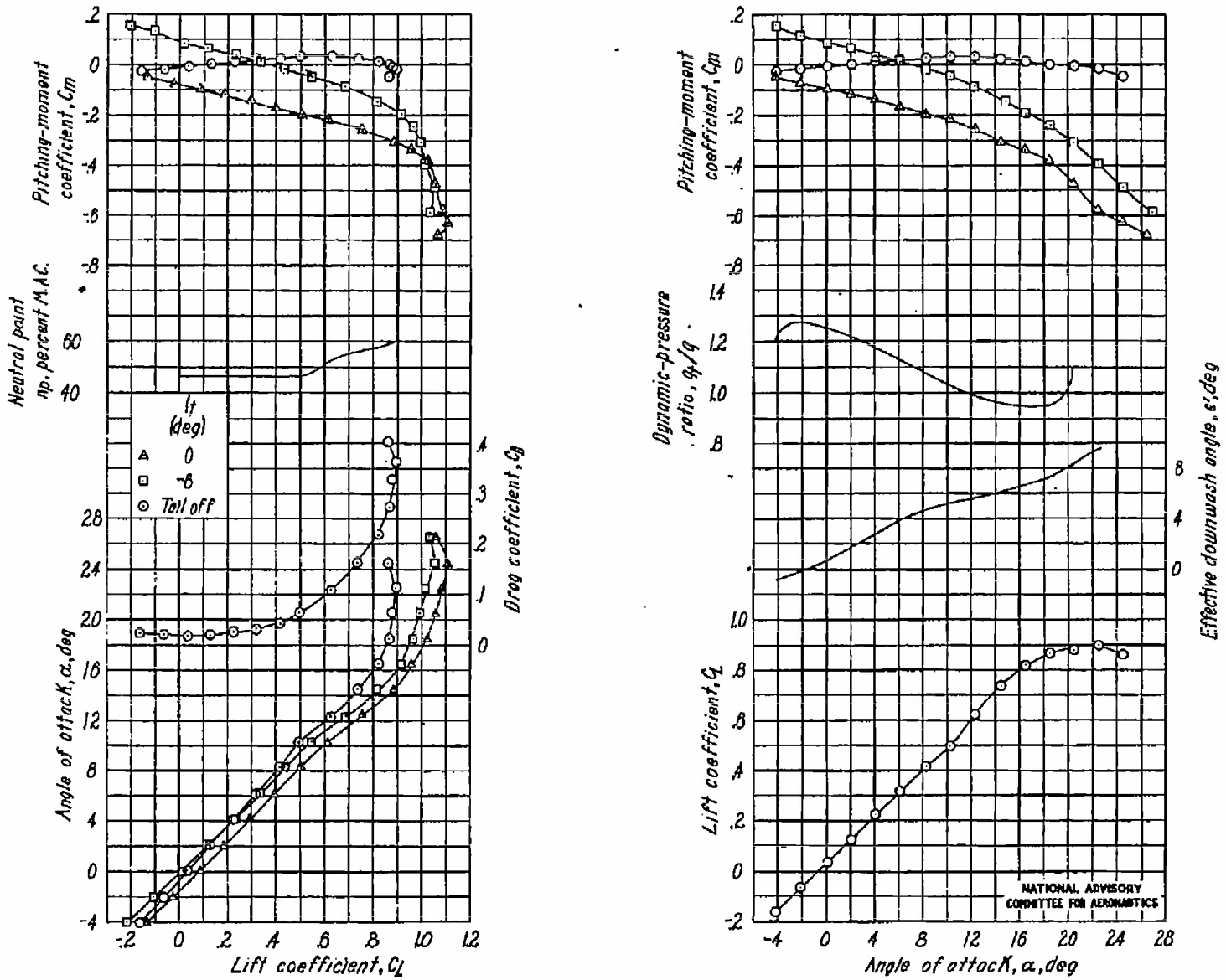


(f) Position 6.

Figure 15.- Concluded.

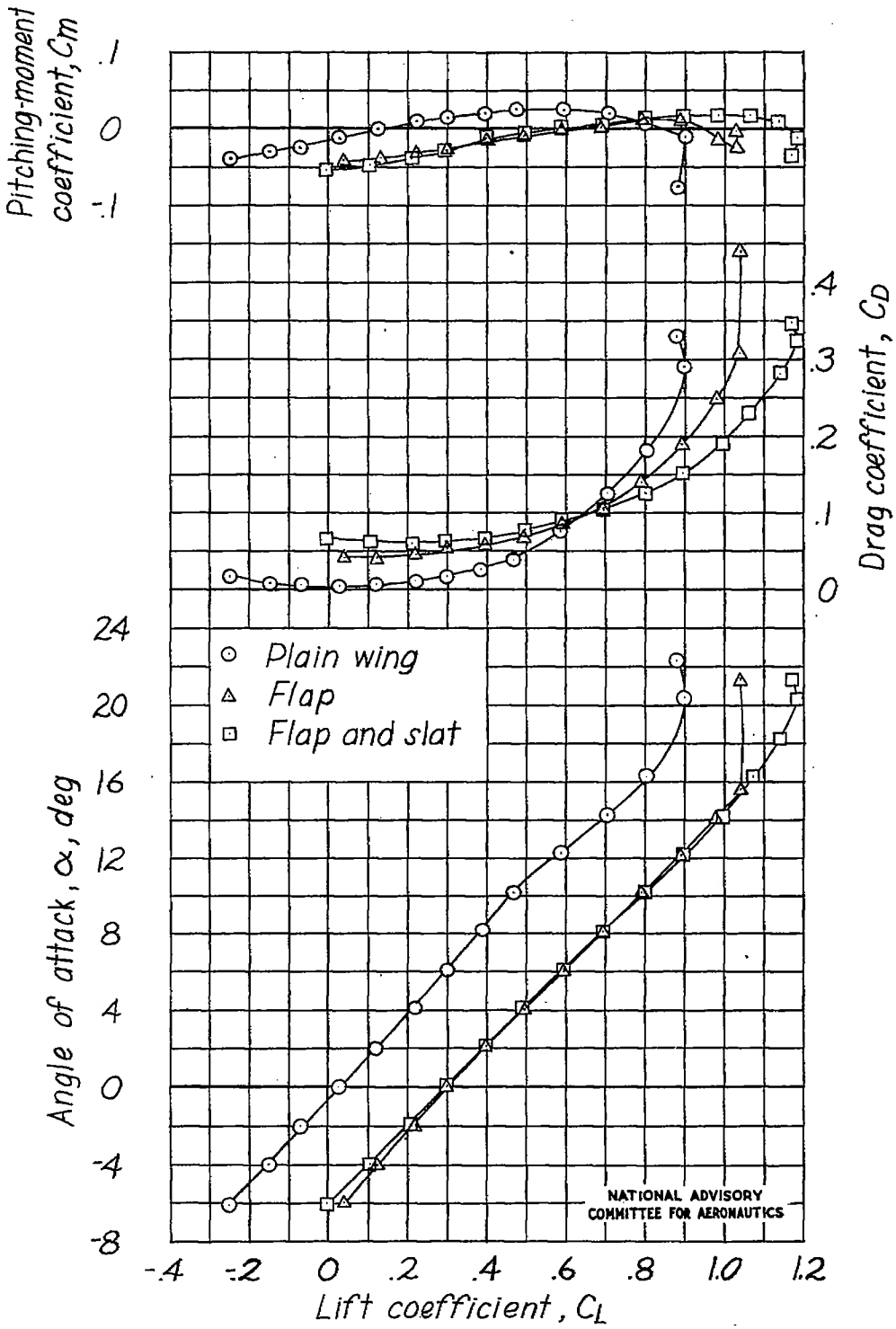


Figure 16.- Aerodynamic characteristics of wing of model D equipped with high-lift devices. $\frac{c_R}{c_T} = 0.617$; $A = 3$; $\Lambda_{c/4} = 37.5^{\circ}$.

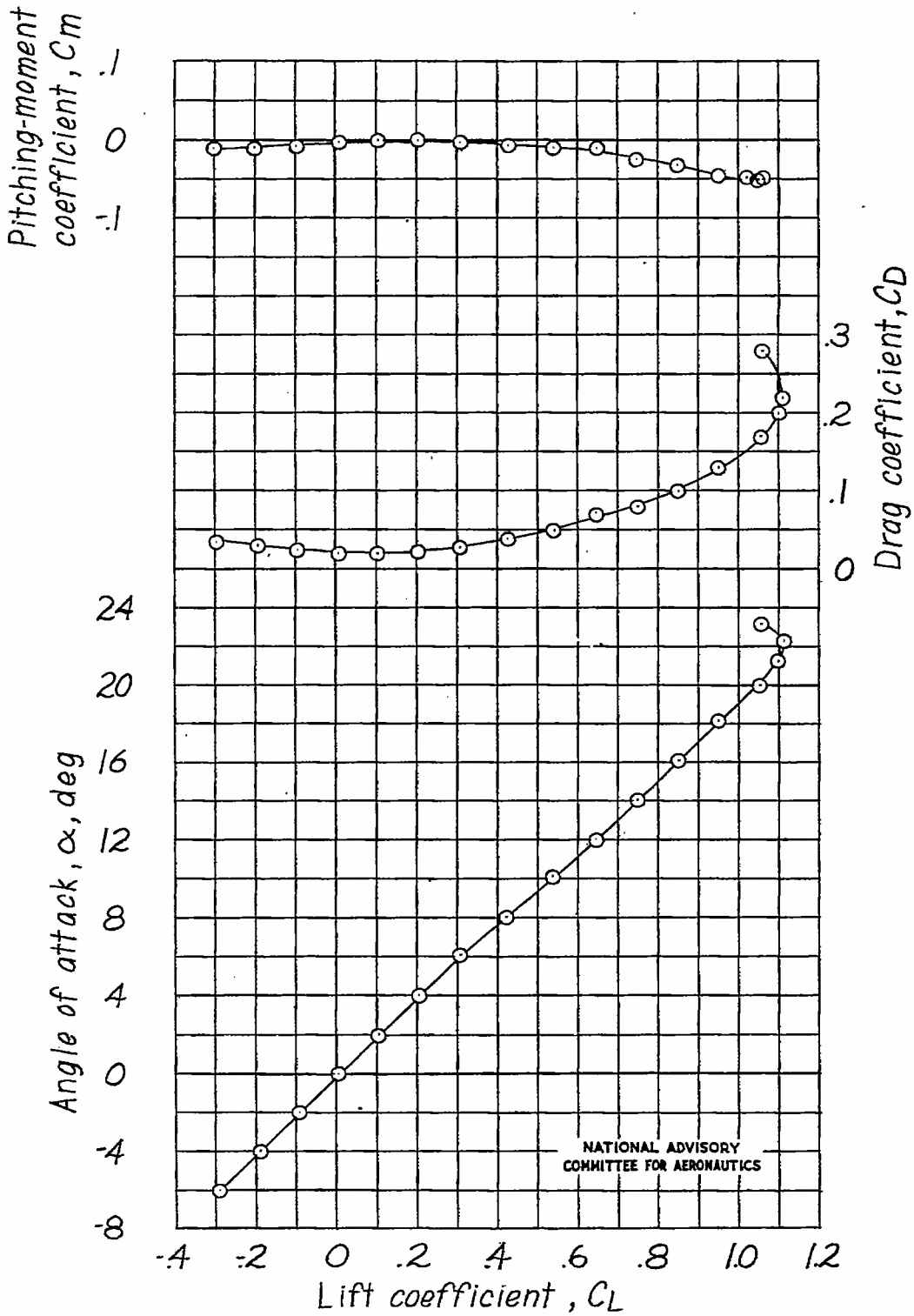


Figure 17.- Aerodynamic characteristics of model E. $\frac{c_R}{c_T} = 2.04$; $A = 3$; $\Lambda_{c/4} = 37.5^{\circ}$.

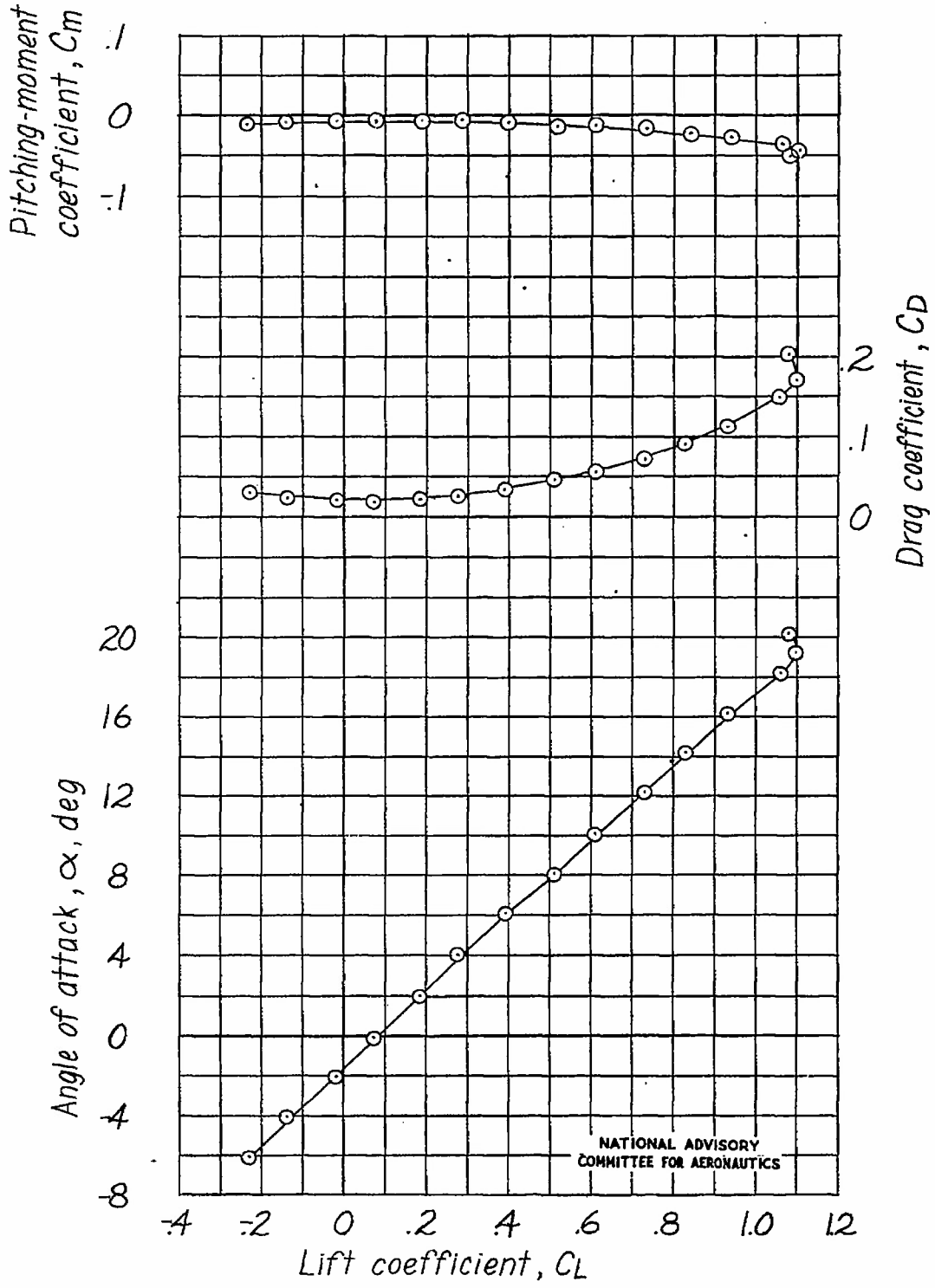


Figure 18.- Aerodynamic characteristics of model F. $\frac{c_R}{c_T} = 2.06$; $A = 3.3$; $\Lambda_{c/4} = 32.5^{\circ}$.

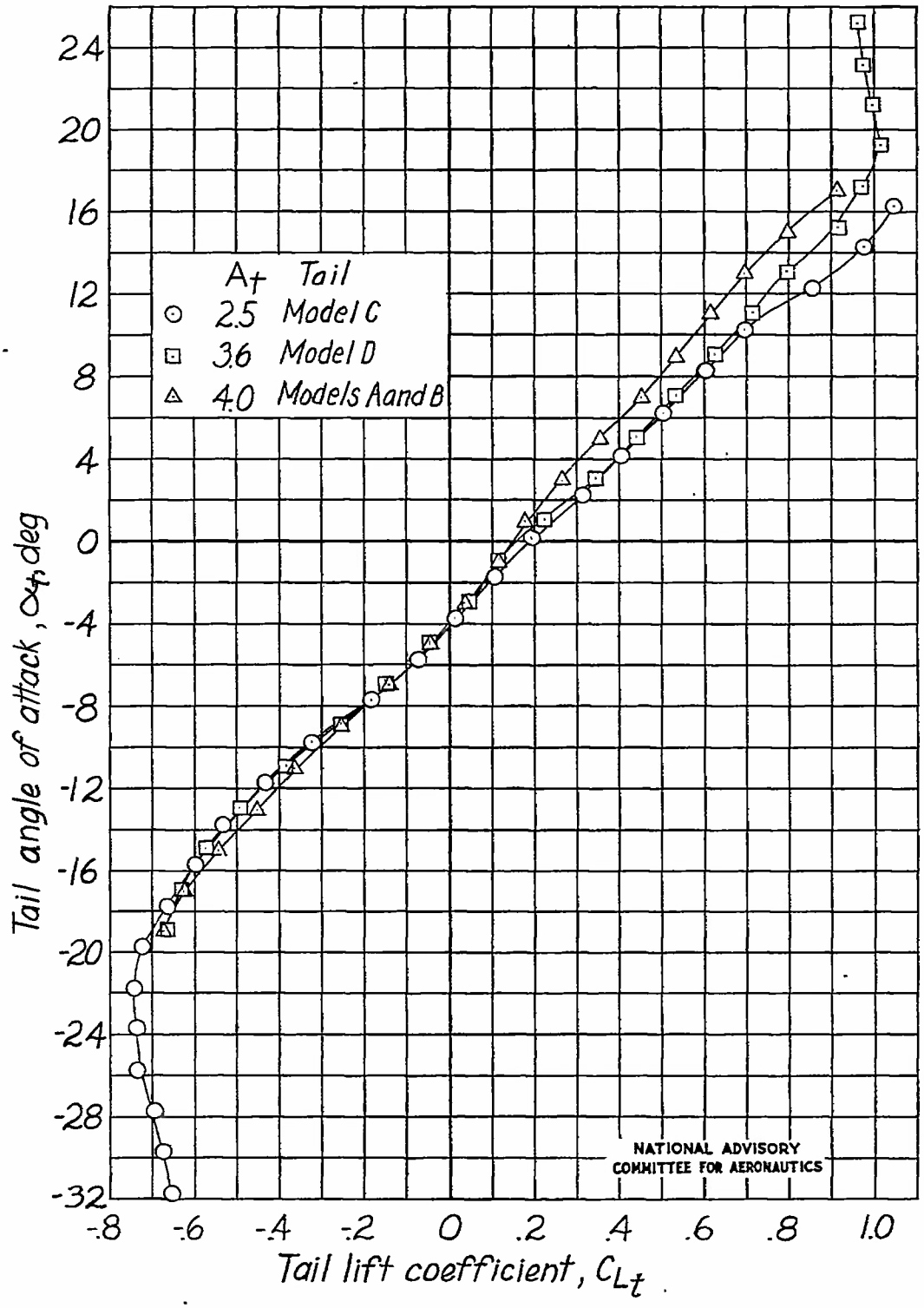


Figure 19.- Characteristics of isolated horizontal tails. $\frac{c_R}{c_T} = 1.0$; $\Lambda_{c/4} = 40^\circ$. Clark Y airfoil section.

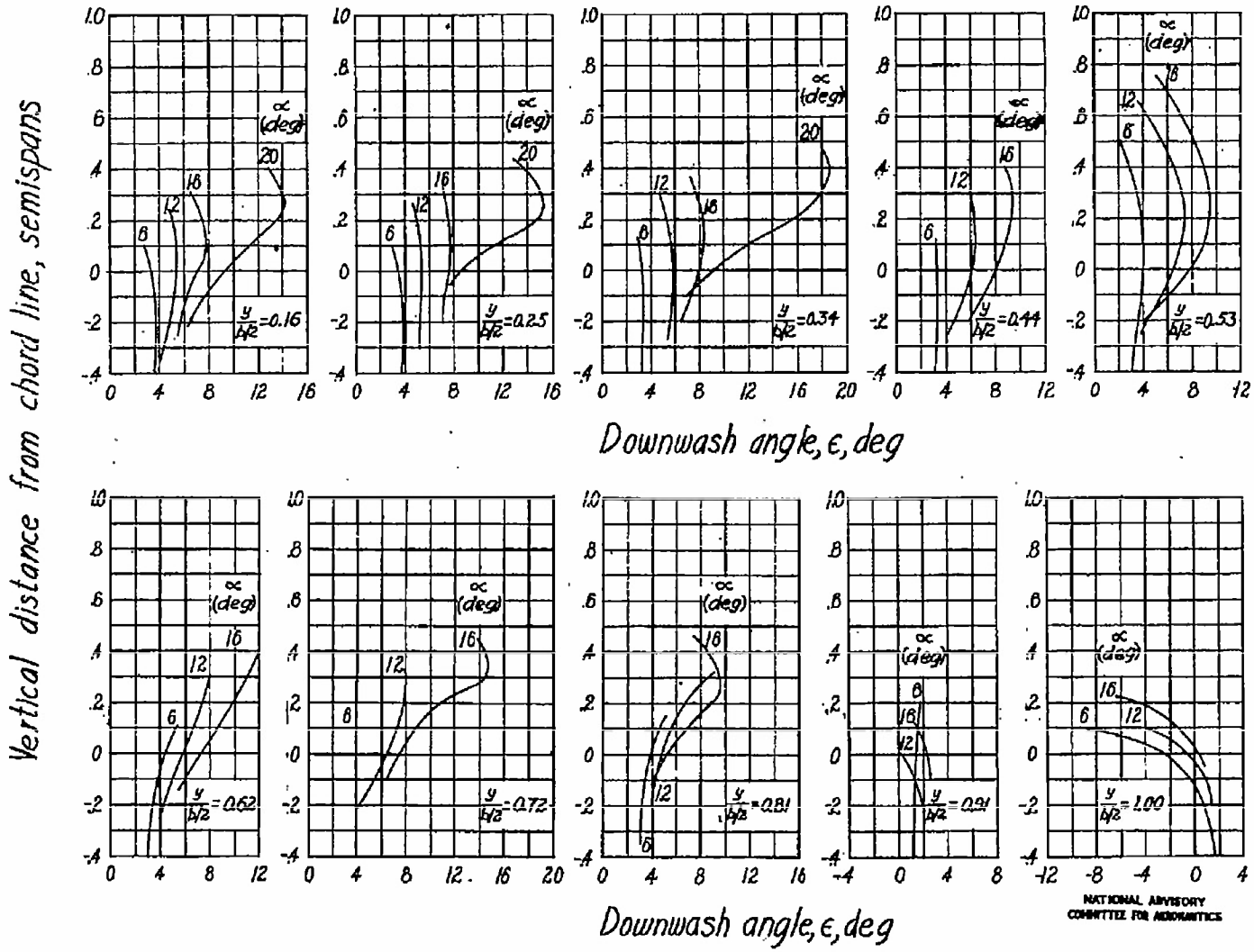


(a) $\frac{l_t}{b/2} = 1.5$.

Figure 20.- Tuft surveys behind models B and C with tail removed.

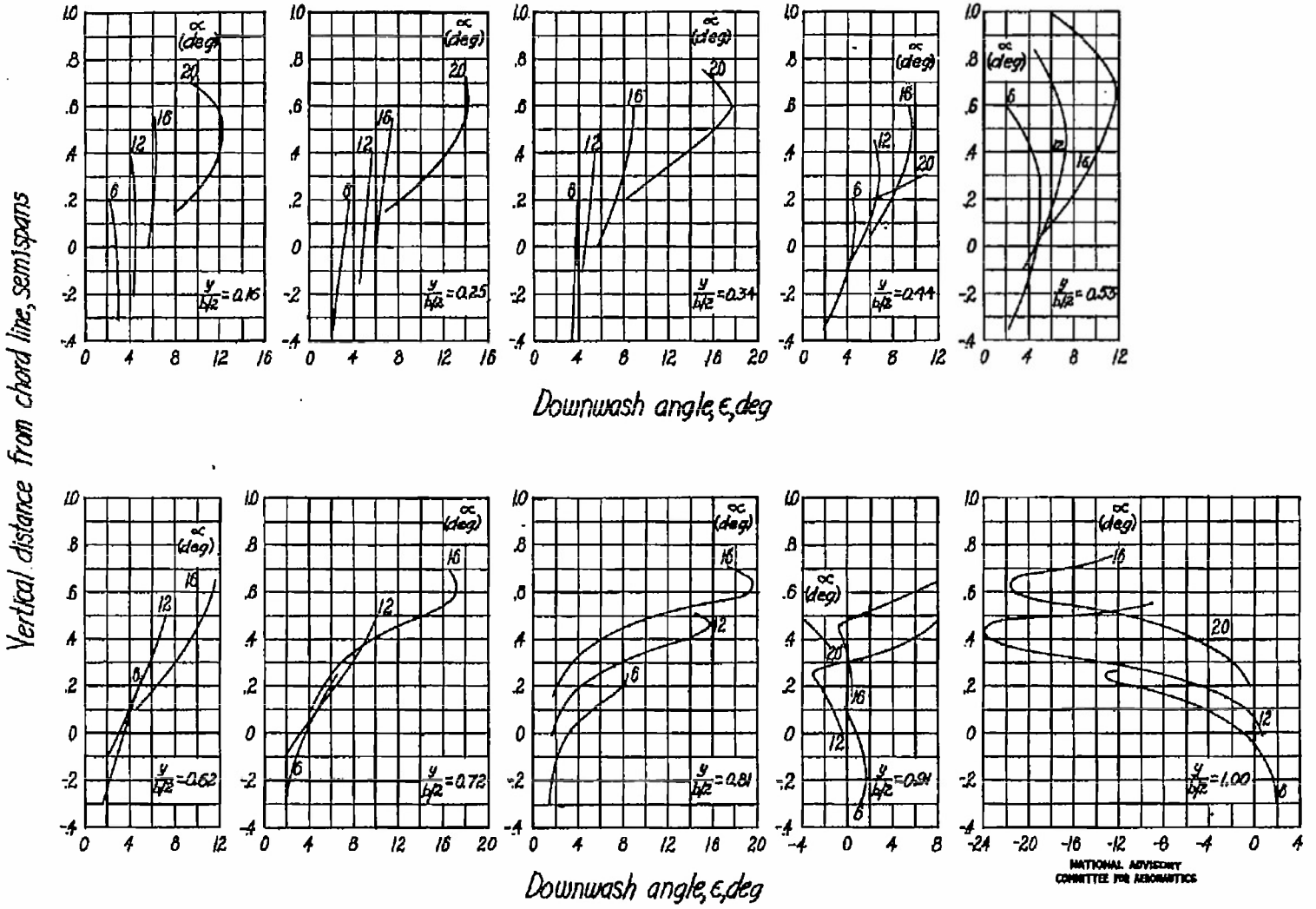


(b) $\frac{l_t}{b/2} = 2.3.$

Figure 20.- Concluded.

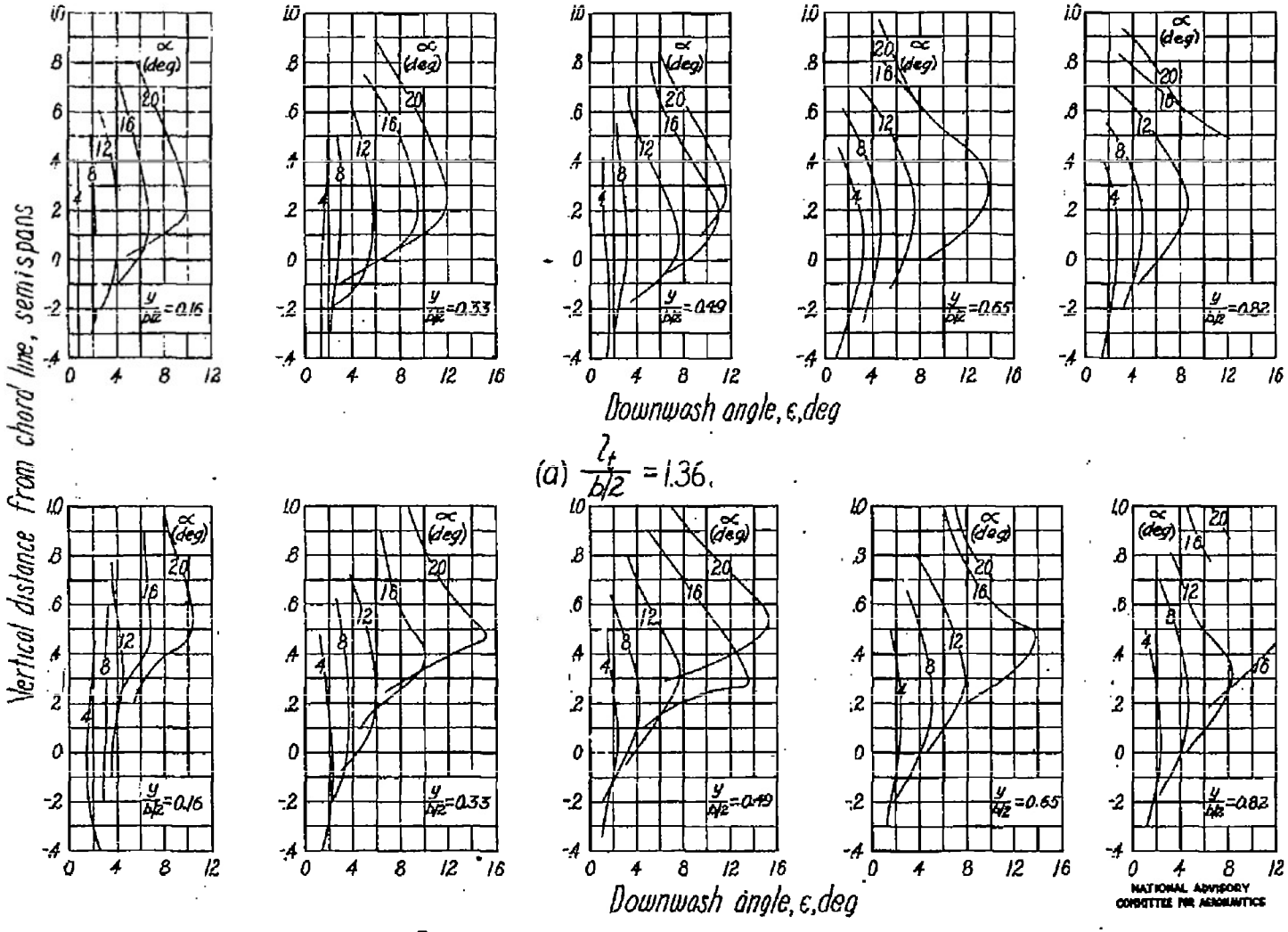


(a) $\frac{l_t}{b/2} = 1.36.$

(b) $\frac{l_t}{b/2} = 1.91.$

Figure 21.- Tuft surveys behind wing of model D.

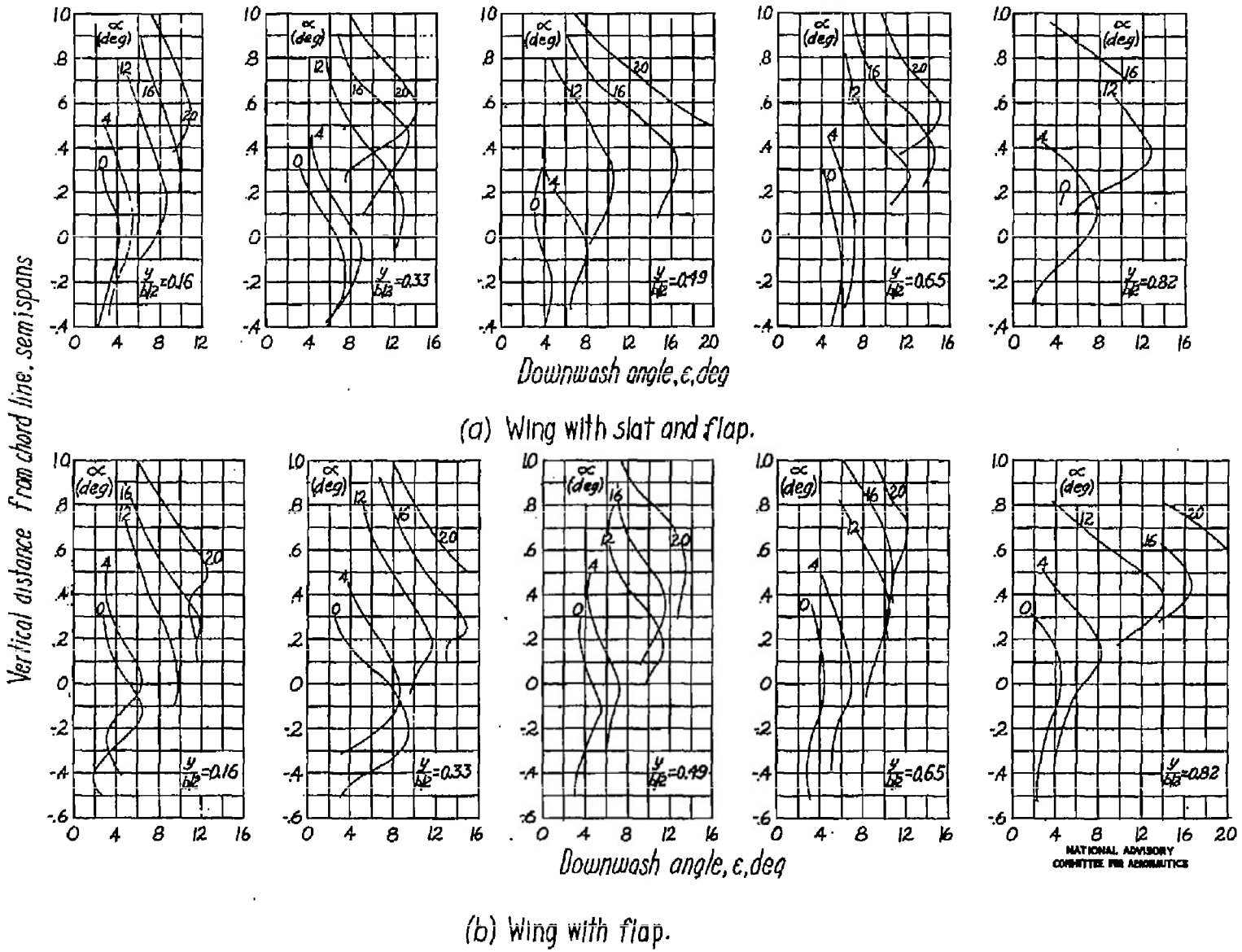


(a) Wing with slat and flap.

(b) Wing with flap.

Figure 22.- Tuft surveys behind wing of model D equipped with high-lift devices. $\frac{l_t}{b/2} = 1.91$.

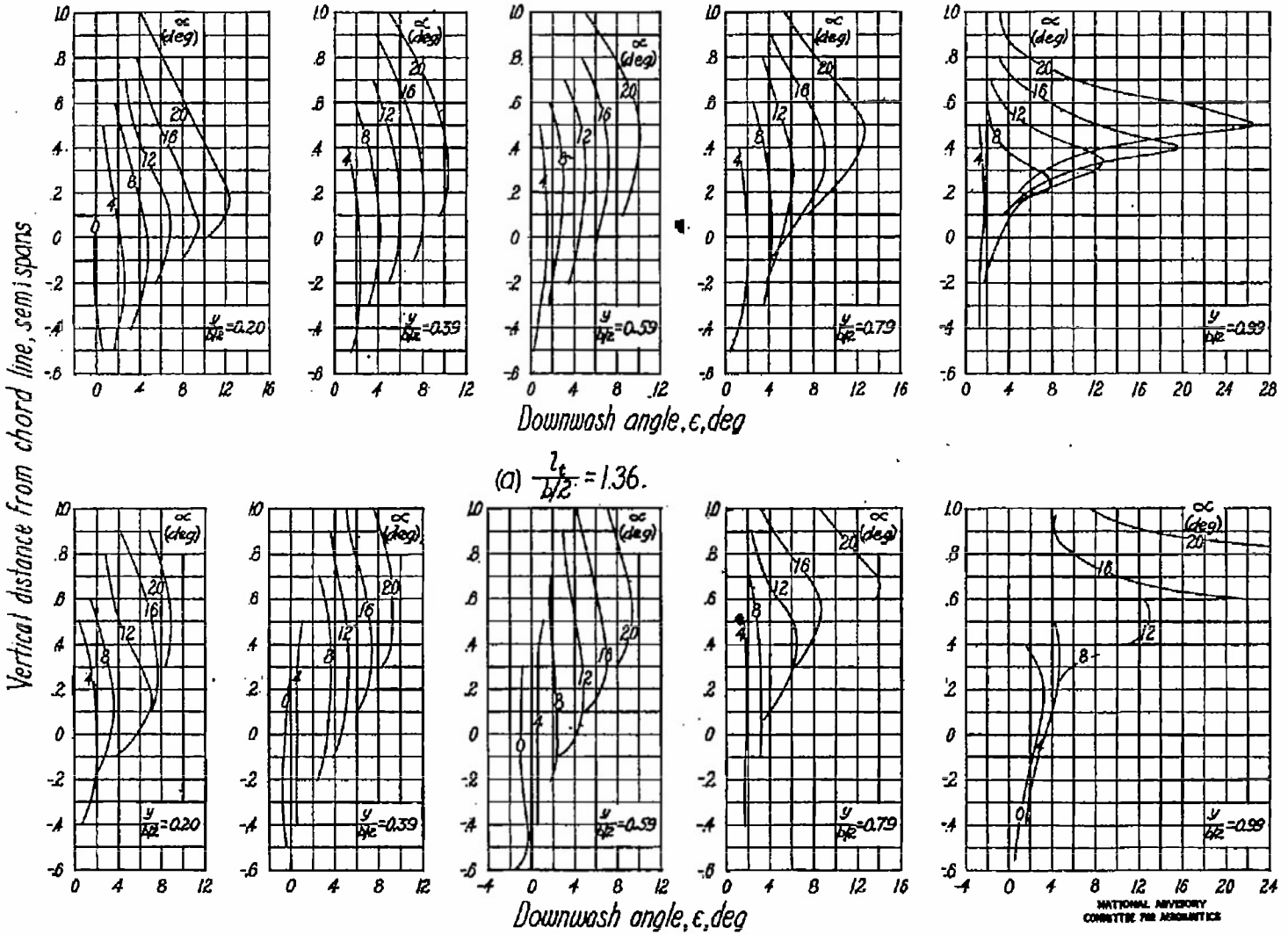


(a) $\frac{l_t}{b/2} = 1.36.$

(b) $\frac{l_t}{b/2} = 2.03.$

Figure 23.- Tuft surveys behind model E.

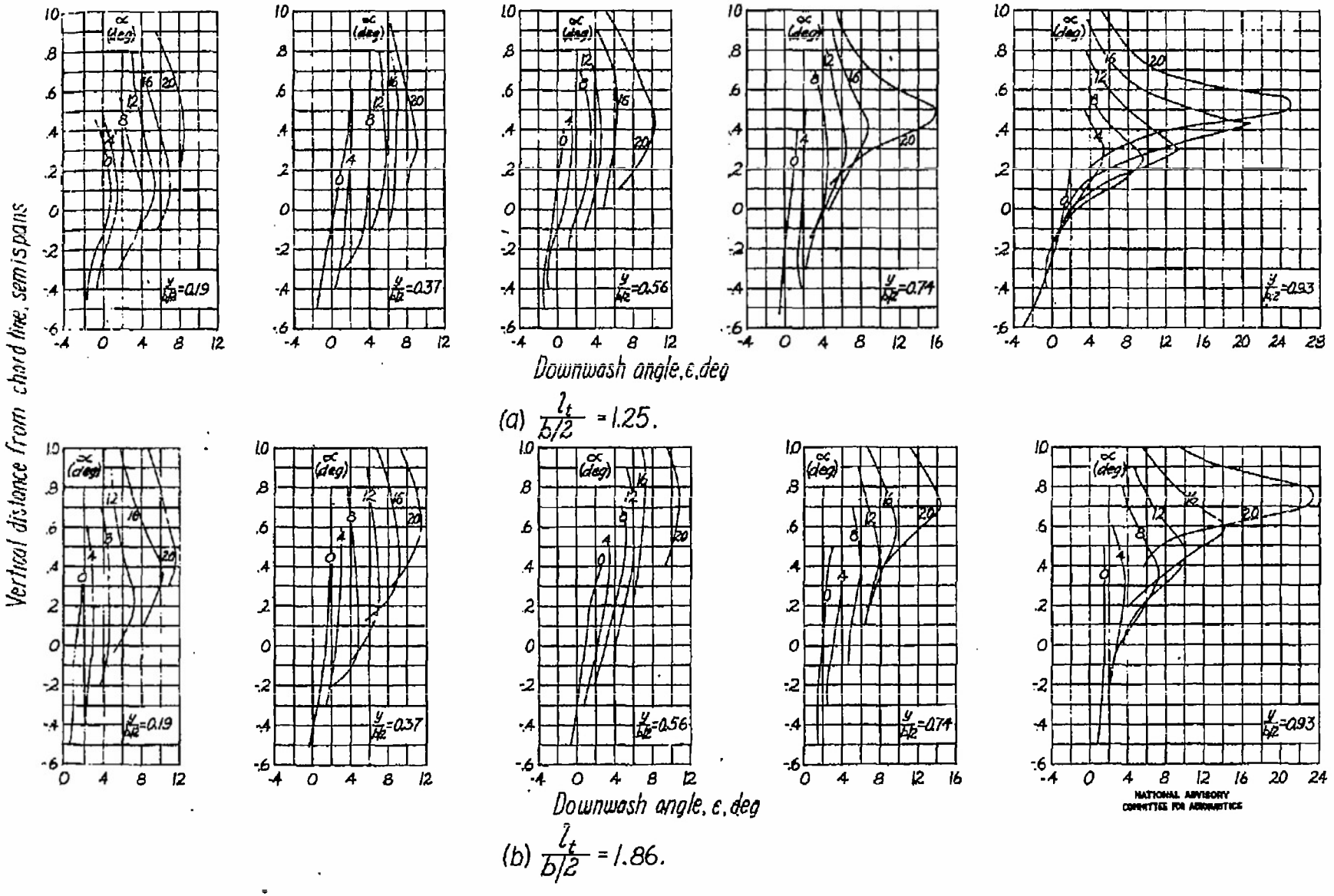


Figure 24.- Tuft surveys behind model F.

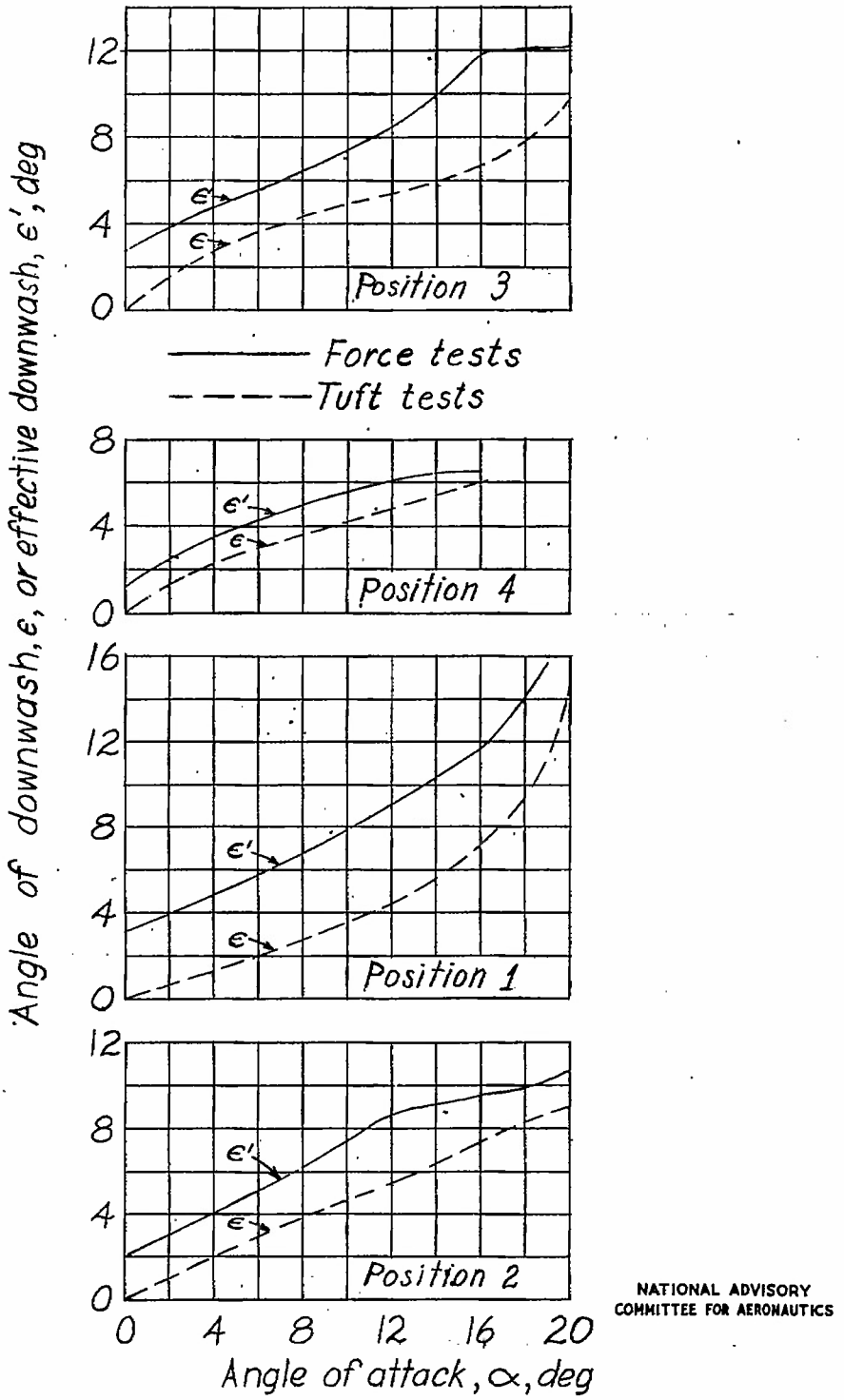


Figure 25.- Comparison of values of downwash angles determined by tuft and force tests. $\frac{c_R}{c_T} = 1.0$; $A = 2.5$; $\Lambda_{c/4} = 40^\circ$. Model C. $b_t = 0.5b$. Tufts at $y = 0.25\frac{b}{2}$.

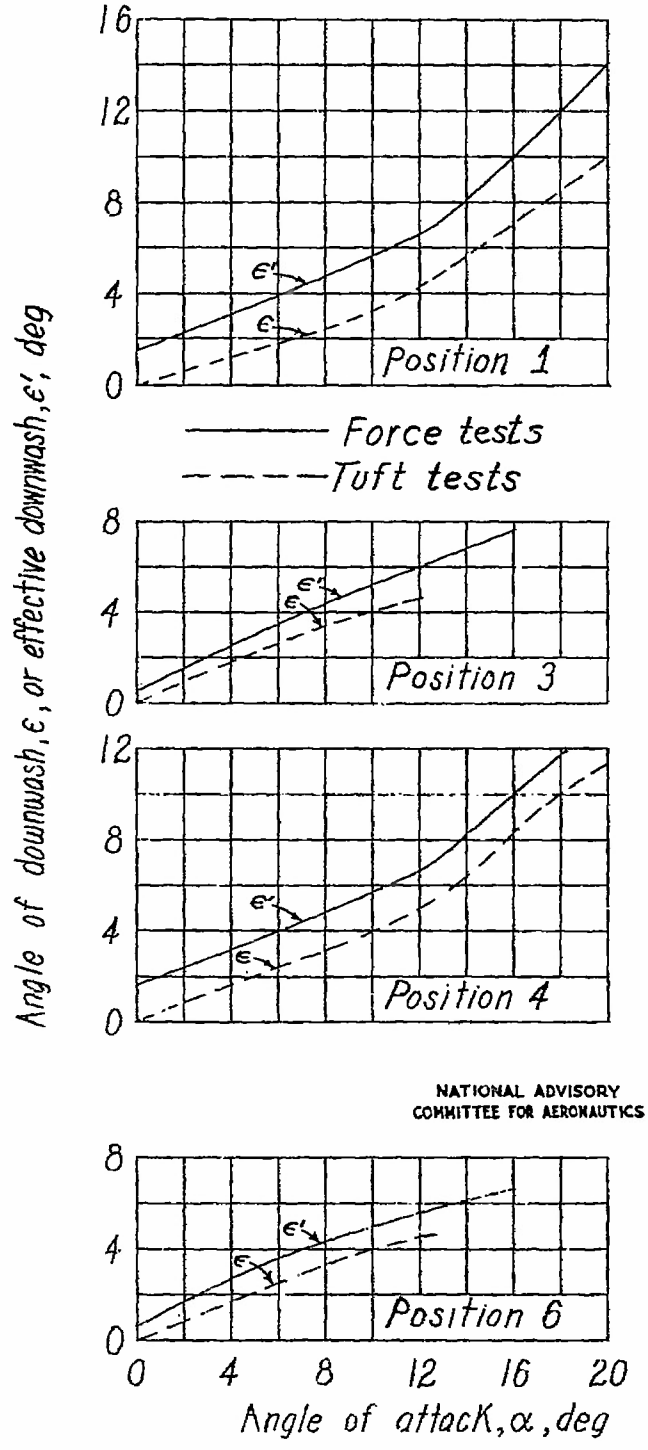


Figure 26.- Comparison of values of downwash angle determined by tuft and force tests. $\frac{c_R}{c_T} = 0.617$; $A = 3.00$; $\Lambda_{c/4} = 37.5^\circ$. Model D. $b_t = 0.5b$. Tufts at $y = 0.25\frac{b}{2}$.

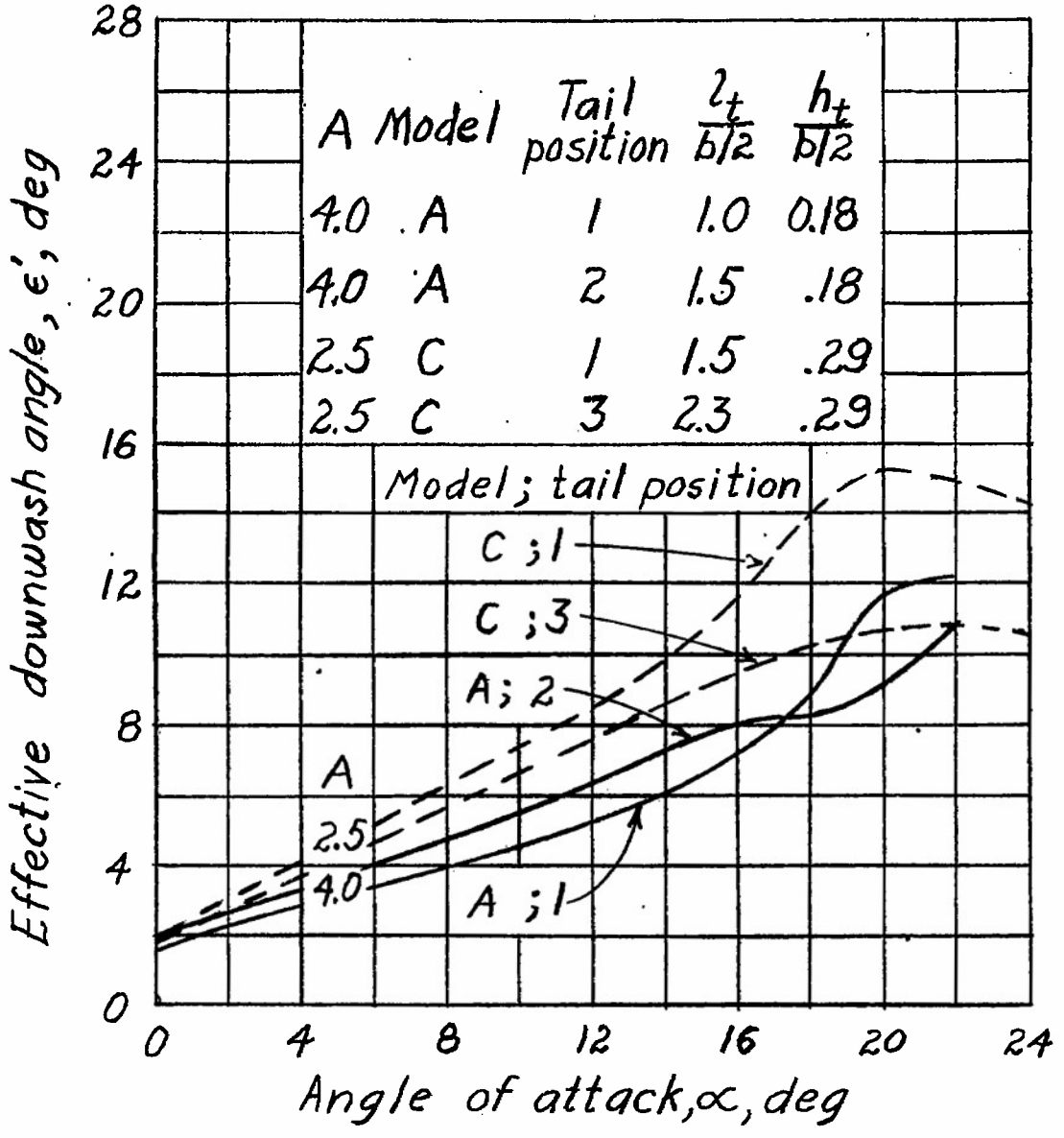


NATIONAL ADVISORY
COMMITTEE FOR AERONAUTICS

Figure 27.- Effect of wing aspect ratio on effective downwash angle behind sweptback wings. Models A and C. $\frac{c_R}{c_T} = 1.0$; $\Lambda_{c/4} = 40^\circ$.

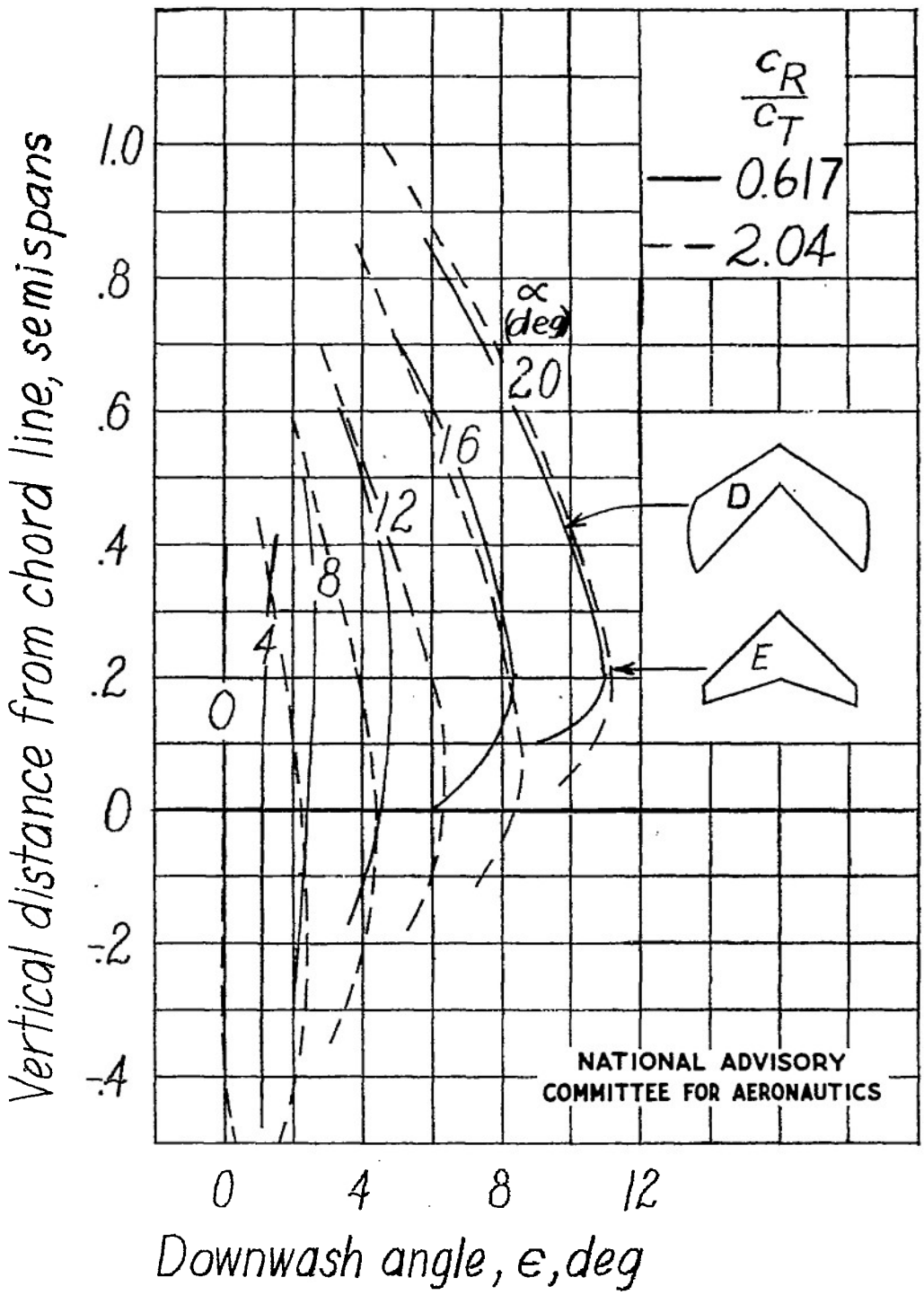


Figure 28.- Effect of taper ratio on downwash angle behind sweptback wings of models D and E. $\Lambda_{c/4} = 37.5^{\circ}$; $A = 3$; $l_t = 1.36\frac{b}{2}$; $y = 0.25\frac{b}{2}$.

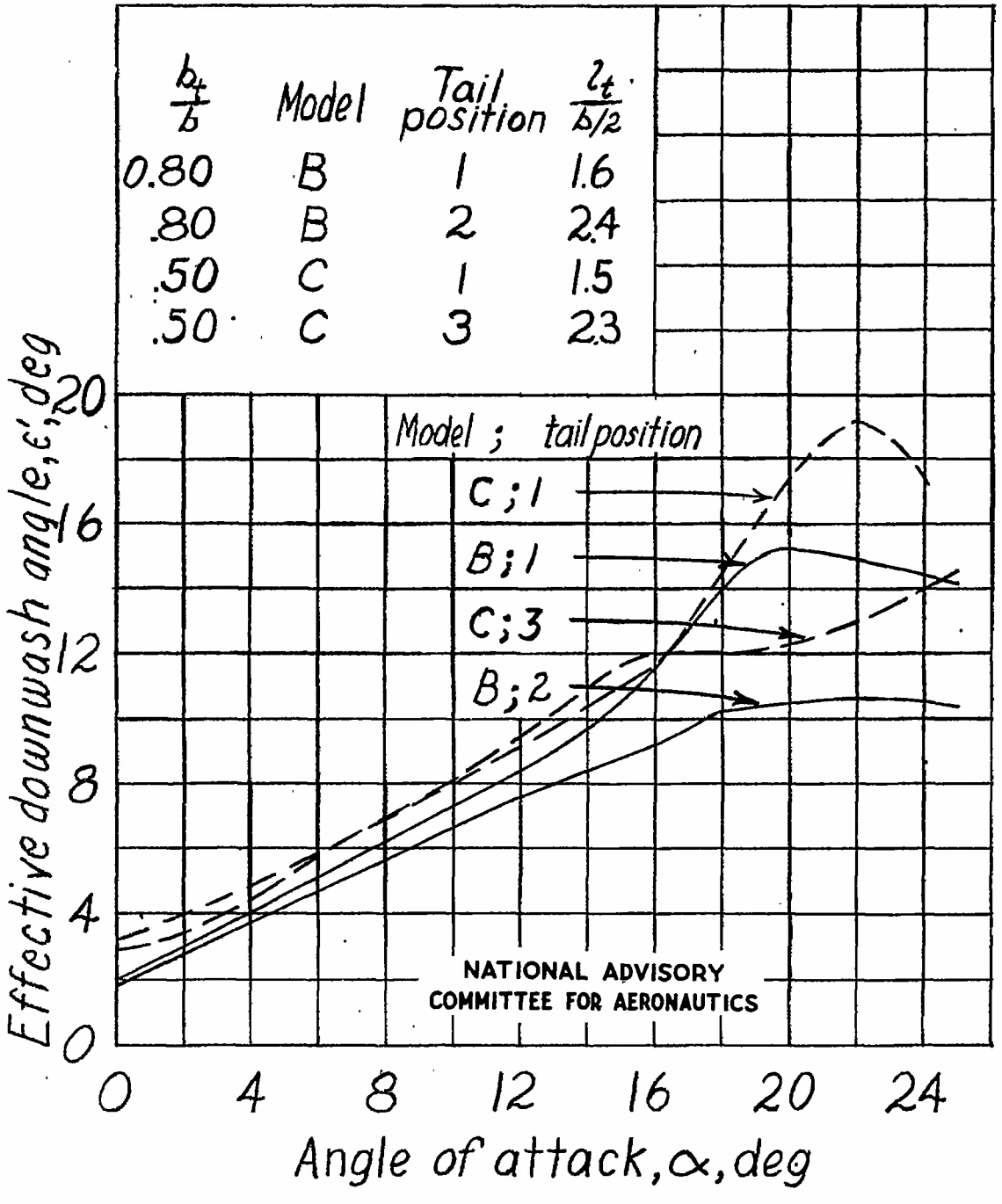


Figure 29.- Effect of tail span on effective downwash angle behind sweptback wings. Models B and C. $\Lambda_{c/4} = 40^{\circ}$; $A = 2.5$; $\frac{c_R}{c_T} = 1.0$; $h_t = 0.29\frac{b}{2}$.

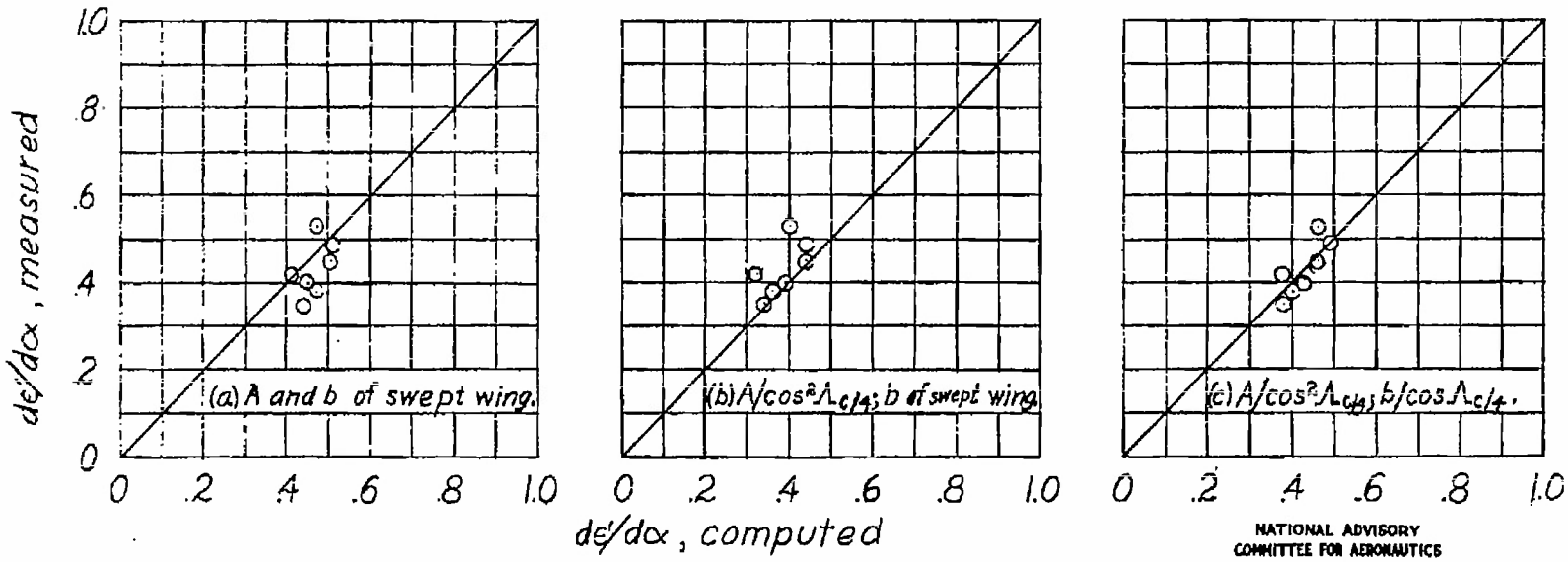


Figure 30.- Comparison of measured and computed values of $d\epsilon/d\alpha$ for sweptback wings.

AD-B804 048

ertaining to classified will be found added to the a

ATI FORM (19 Oct 47)

Purser, Paul E.
Spearman, L. M.
Bates, W. R.

AUTHOR(S)

DIVISION: Aerodynamics (2)
SECTION: Stability and Control (1)
CROSS REFERENCES: Stability (89100); Airfoils - Downwash (08100)

ATI- 9574
ORIG. AGENCY NUMBER
TN-1378
REVISION

AMER. TITLE: Preliminary investigation at low-speed of downwash characteristics of small-scale sweptback wings

FORG'N. TITLE:

ORIGINATING AGENCY: National Advisory Committee for Aeronautics, Washington, D. C.

TRANSLATION:

| COUNTRY | LANGUAGE | FORG'N.CLASS | U. S.CLASS. | DATE | PAGES | ILLUS. | FEATURES |
|---|---|---|---|---|---|---|---|
| U.S. | Eng. | | Unclass. | Jul'47 | 55 | 30 | photos, diagrs, graphs |

ABSTRACT

Test results show that lowering the tail to the extended wing chord lina and increasing tail length improved etability characteristics and decreased stability variations with larga angles of attack. Increasing wing aspact ratio reduced $d\epsilon/d\alpha$ and improved tail contribution to stability. Trailing edge flaps decreased $d\epsilon/d\alpha$ slightly. Leading edge flaps reduced $d\epsilon/d\alpha$ variation at high lift coefficient and improved stability characteristics. Design chart downwash angle values for unswept wings agreed fairly well with experimental data.

NOTE: Requests for copies of this report must be addressed to: N.A.C.A., Washington, D. C.



U7-0-21 MAR 47